

# Reply to Comments made by RC 1.

Note that the reply is in bold.

Review of “Droplet clustering in shallow cumuli: The effects of in-cloud location and aerosol number concentration” by Dodson and Small-Griswold submitted to Atmospheric Chemistry and Physics (ACP).

**We would like to start by addressing concerns raised by both of the Referees. First, we apologize for the delayed response and posting of the revised manuscript. We put in a great deal of time and effort to do a rewrite of the paper, to shift the focus from the smaller scale clustering originally discussed to larger scale mixing as a result of entrainment. Both Referees raised concerns that the PCFs examined are more closely related to entrainment mixing as compared to preferential concentration, and we have also come to that conclusion. In particular, our PCF spatial scale does not extend into the Kolmogorov range, suggesting that inertial clustering (if present at all) isn't being measured. Our PCF curves also mirror those presented in Good et al. (2012) and Ireland and Collins (2012), which used the PCF for the purpose of analyzing larger-scale clustering due to entrainment mixing. Lastly, we have de-normalized all PCF curves displayed throughout the manuscript. In Saw et al. (2012) the PCF curves are normalized at the range the larger scale inhomogeneous mixing is occurring (i.e., the ‘shoulder’ region of the curve). Since the ‘shoulder’ region of the curve is what we are analyzing, normalizing it to a common value becomes unreasonable.**

Recommendation: reject and encourage resubmission

General evaluation: This paper reports analysis of observations applying a statistical technique that aims at documenting cloud droplet clustering. I found this subject interesting and fitting the ACP scope. However, I am confused by the specific detail of the analysis (PCF normalization) and I feel the way analysis is performed amounts to throwing the baby out with the bathwater. Specifically, forcing the PCF to approach zero at large scale is not appropriate as there are likely large-scale heterogeneities both at the cloud core (i.e., due to different updraft across the cloud base and thus fluctuations of cloud droplet concentrations above) and at cloud edges due to turbulent mixing and filamentation. I have to admit that I started to read the paper with large expectations, and my enthusiasm went down and down as I kept reading. I admit that I stopped reading at the end of section 4.1. I do feel that the analysis is flawed because of the normalization that forces the cloud to look homogeneous at large scales. There are plenty of cloud observations

showing that such an assumption is simply not valid! Thus, I recommend the paper to be rejected and then resubmitted with the discussion based on PCFs without normalization. There are numerous other problems and their sheer number (see specific comments) also suggests the need for a significant rewriting.

**We have realized through your comment that a more clear discussion/explanation of the normalization process was needed. In responses to your other comments that deal with the normalization we will give a more detailed explanation. However, because we have de-normalized all PCF functions in the new manuscript, normalization no longer applies. To clarify a few things however, we were not attempting to say that there were not large-scale heterogeneities within the cloud. We were simply accounting for said heterogeneity by adjusting all PCF curves to a common value at larger scales (as is done in Shaw et al. (2002), with a much better explanation of the normalization coming in Saw et al. 2012)).**

Major comments:

1. This comment is arguably more to the ACP technical staff than to the authors. The collection of figures at the end of the manuscript is unacceptable: figures are way too small and the only way to review their details is to go to the electronic version of the paper and zoom in. I feel the journal staff should request the authors to revise the submission before publishing the paper online to have each figure legible (e.g., one figure per page).

**We used the Latex Template that is available through the ACP website. To account for the figures, we adjusted the input parameters to make the figures bigger in the new manuscript. Hopefully this will account for the problem.**

2. I do not feel the introduction is appropriate. First, it touches on some issues only remotely related to the specific focus of the paper (e.g., the indirect effects). The selection of references is incomplete or simply inappropriate. Second, the review of previous studies concerning clustering misses important publications as there are studies showing relatively small clustering (in contrast to the papers cited right now). Overall, I agree that there is likely some clustering at the cloud microscale, but its magnitude is relatively small and thus difficult to extract from observations.

**We have completely rewritten the introduction by shifting the focus from the small scale inertial clustering to clustering caused by entrainment mixing. We have made an attempt to include and remove references as you recommended in the following comments. We have mentioned that not all studies have measured clustering (see page 3 lines 14-17 in the new**

**manuscript) by citing Chaumat and Brenguier (2001). Although we do not elaborate much, readers will at least come to the realization that not all studies have measured inhomogeneities.**

3. The discussion in the introduction and in section 2.1 excludes the impact of gravitational acceleration on droplet clustering. This is a serious omission as I would argue that droplet sedimentation is the mean reason for a relatively small droplet clustering. I provide detailed comments below, the Grabowski and Vaillancourt (1999) comment on Shaw et al. (1998) in particular.

**The original reason we left out a discussion on gravitational acceleration is due to the fact that there is no way to account for it in our observations/data. What we mean is, gravity is a constant in the atmosphere unlike in laboratory experiments where gravity can be accounted for by enhancing or reducing it, as was done in Ireland and Collins (2012). However, you are right that the impact that gravity has is significant, and it is still important for the readers to understand the impacts that gravity has. A discussion on the effects of gravity on droplets has been added on page 5 lines 14-22 of the new manuscript.**

4. The way PCF is calculated (section 2.3) need to be better explained. First, I am not sure why normalization is needed. Second, it is not explained how the normalization is performed (a simple shift?). I think there might be interesting differences between cloud cores and cloud edges due to entrainment and small-scale filamentation for the latter (this is what is illustrated in Fig. 1, correct?) In other words, cloud core and cloud edge may look different at different scales. For instance, near the edges, there may be differences at large scales (say tens of centimeters and meters, see Fig. 1), but similar clustering may take place at small-scales (the latter is the focus of the manuscript, correct?). Moreover, normalizing PCF does not allow estimating the magnitude of small-scale concentration fluctuations. The fact that Shaw et al. (2002) did the renormalization is not convincing (although I had just a quick look at that paper without getting into details). I feel this has a significant impact on the results and their interpretation.

**You are right that a better job needed to be done to correctly explain the normalization process and why it was needed. I think Referee 2's initial comments do a good job of summarizing the findings in Saw et al. (2012). They found that when two clustering signatures (or inhomogeneities) are occurring and are uncorrelated to one another and have a large enough scale separation (such as inertial clustering on the Kolmogorov scale and entrainment induced clustering occurring on cm to tens of meters scale), the PCF**

equals the product of two PCFs, each results from the one of the two clustering phenomena acting alone, i.e.,  $n(t) = n_1(t)*n_2(t)$ .

The resulting PCF curve that is produced when both inertial clustering and larger scale inhomogeneities are present is described on page 6 lines 13-21 of the new manuscript. The curve has a power law region at the smallest scales where inertial clustering is present, followed by a 'shoulder' region that is due to the larger scale inhomogeneity. The curve then falls off towards zero at even larger scales (see Figure 4 in Saw et al. 2012). Figure 5 in Saw et al. 2012 goes on to show how the shoulder region of the curve can be 'normalized' to a common value (in this case a value of one for the Radial Distribution Function, in our case it was zero for the PCF). This then allows for analysis of the clustering at the smaller scales.

With that stated, we do believe that the process by which we did the original normalization was flawed. In particular, we were normalizing the PCF curves at the largest scales where the PCF continues to decrease sharply (the region directly after the shoulder region) in order to analyze the differences in the shoulder region. However, in Saw et al. (2012) the PCF is normalized at the shoulder region in order to compare differences in the inertial clustering. We are unaware of any work that has been conducted which shows PCF normalization is valid at the largest scales in order to analyze the shoulder region scale clustering. Although it has been shown that the PCF can be normalized in the shoulder region to analyze inertial clustering, normalizing the PCF at the largest scales to analyze the entrainment scale clustering may or may not be valid.

Specific comments (those requiring special attention - more serious - marked with \*).

1. P. 1, L. 20. I think it would be appropriate to cite Grabowski and Wang (2013) that reviewed the progress in this area a decade after Shaw (2003).

**We have kept the original reference of Shaw (2003) but have also added Grabowski and Wang (2013). This section of text now occurs on page 1 line 25 to page 2 line 2.**

2. P. 1, bottom paragraph: This is a very pessimistic message. I think there are many realistic cloud simulations showing relatively fast rain formation (e.g., vanZanten et al. 2011, Seifert et al. 2010, Wyszogrodzki et al. 2013, Khain et al. 2013).

**The original idea with this was to motivate why droplet clustering is so important, since**

**classical droplet growth theory does such a poor job of estimating the rain formation time. This discussion now appears on page 2 line 4-8. The references you mention have been added on page 2 line 8-11 to state that progress has been made in modeling precipitation. However, we also state that improvements still need to be made, as is mentioned in Wyszogrodzki et al. (2013).**

3. P. 2, L. 5: Earlier references than Khain and Lehman would be appropriate here. For instance, the exchange between Telford and Chai on one side and Jonas and Mason on the other in QJ in 1983 is worth referring to (the great phrase comparing the impacts of entrainment to turning down the gas to boil water faster!). Perhaps some papers of Charlie Knight at about the same time are also of relevance.

**Entrainment is first mentioned on page 2 lines 11-13 of the new manuscript, and includes the references of Telford and Chai and Jonas and Mason. Since the focus of the paper has been shifted from inertial clustering to clustering caused by entrainment, an extensive discussion on entrainment is given on page 2 lines 22-29 and page 4 lines 13-32 which includes references of some of the earlier work on entrainment, including Warner (1969) on page 2 line 12 and Baker (1980) on page 2 line 24.**

4. P. 2, L. 6: For GN and UGN, there is the Illingworth (1988) paper way before the Knight et al.

**The discussion on GN and UGN has been completely removed from the new manuscript.**

5. P. 2, L. 8: “no one theory” is simply incorrect, please see 2 above.

**We were not trying to imply that none of the theories are correct. We were implying that it is most likely a combination or all of the theories that account for the fast formation of rain that is observed. With that said however, this statement has been removed. And the discussion on the different theories on the fast formation of rain which originally occurred on page 2 lines 3-7 (such as turbulent deviations of supersaturation and GN and UGN) has also been removed to just focus on entrainment mixing and droplet clustering.**

6. P. 2, L. 9-18: this paragraph should be deleted as irrelevant to the results presented. Referring to Small et al. (2009) rather than to original papers (Twomey, Albrecht, etc.) is simply inappropriate. Also, Xue and Feingold (JAS 2006) is a more appropriate first reference to the impact of cloud-edge evaporation impact.

**This paragraph has been modified in accordance with your comments. We have included**

**Xue and Feingold (2006) which is a modeling experiment, but have also kept Small et al. (2009) since this is an in-situ experiment. Any mention of direct and indirect effects have been removed from the paragraph (which we do agree is irrelevant, especially with how the manuscript has been refocused). However, the mention of the evaporation-entrainment feedback is important, as it explains why we would expect to see enhanced entrainment (and as a result enhanced clustering) for the high pollution clouds as compared to the low pollution clouds. This paragraph can now be found on page 2 lines 16-21 of the new manuscript.**

7\*. P. 2, L. 19-26: Brenguier and Chaumat (2001) has to be cited here to show that not all studies indicate significant clustering at small scales! In fact, I would argue that the clustering is relatively small (e.g., see Fig. 3 in Kostinski and Shaw 2001 and Fig. 5 in Vaillancourt et al. 2002).

**A brief discussion on the findings of Brenguier and Chaumat (2001) are given on page 3 lines 14-16 of the new manuscript. We also report that not all of the clustering measured shows a statistical difference from a random distribution. In particular see page 9 line 29 to page 10 line 10 of the new manuscript. Also see page 14 lines 1-5, where we state that 31.7 percent of the data we measure (cloud traverses) are randomly distributed.**

8. P. 2, L. 34: there are many more references than Pinsky pointing out to the significance of droplet clustering for collision/coalescence. Perhaps as reference to a review by Grabowski and Wang (2013) would be appropriate here.

**The quantitative results that were previously discussed have been removed (page 2 lines 30-33 in the original manuscripts) since this is beyond the scope of the current manuscript. It is important that the readers understand how droplet clustering can effect collision coalescence in a conceptual manner however. Page 3 lines 10-13 of the new manuscript have added to Grabowski and Wang (2013) reference in relation to how droplet clustering effects collision-coalescence.**

9\*. P. 2, L. 35. I do not think the impact of the Reynolds number (i.e., the range of spatial scales) is important for droplet clustering at the microscale. However, the difference in the eddy dissipation rate between laboratory experiments and natural clouds is the key. That was pointed out by Grabowski and Vaillancourt (1999) who also discuss the role of droplet sedimentation and referred to observations that were subsequently reported in Brenguier and Chaumat (2001). Discussion of the latter aspect, droplet sedimentation, is completely missing from the

manuscript.

**We would agree that the dissipation rate is much more important than the Reynolds number (both for smaller and larger scale clustering), especially since the Stokes number depends on the dissipation rate. The original comment related to the Reynolds number has been removed. We mention the Reynolds number on page 5 lines 22-26 of the new manuscript, stating that it has been found that large scale clustering does not appear to depend on the Reynold's number as is stated in Ireland and Collins (2012). Note that we still mention the physical mechanisms that small scale clustering depends on. It is important to distinguish the physical differences between small scale inertial clustering and larger scale clustering as a result of entrainment mixing.**

10\*. P. 3, last paragraph of the introduction. I think the introduction should lead to the questions posed in this paragraph. The way introduction is written right now does not do that. For instance, why one should expect clustering to depend on the aerosol concentration? Because clustering is expected to depend on the droplet size. Why it should be different between cloud edge and cloud center? Is that because of the droplet size (arguably smaller at the cloud edge) and intensity of the turbulence (larger at the edges)? Similar for the dependence of the distance from cloud base. Etc. Etc. I feel a complete rewrite of the introduction addressing all points above and leading to these questions is needed.

**We believe the points that you have made here have been met in rewriting the new manuscript. For example, after each of the questions proposed at the end of the introduction, a hypothesis is given which an explanation of why said hypothesis was formed. For example, question 3 on page 3 lines 31-32 states that “it is hypothesized that an increase in aerosol load leads to enhanced clustering due to the resulting increased entrainment from smaller droplet sizes and evaporation”. The background information on the reasoning this hypothesis is formed is found on page 2 lines 16-21 of the new manuscript.**

11. P. 3, L. 23: Kolmogorov scale is around 1 mm in atmospheric turbulence.

**This has been corrected in the new manuscript, as seen on page 2 lines 31-32.**

12. P. 4. Eq. (1) is valid only for the case without gravity, correct? If so, it is not appropriate for cloud droplets.

**Yes, Eq. (1) was valid only for the case without gravity. This equation has been removed**

**from the revised manuscript.**

13. P. 4, center: the discussion here should include the effects of droplet sedimentation, see Grabowski and Vaillancourt (1999) and perhaps other papers (e.g., from Prof. Lian-Ping Wang?).

**A discussion on droplet sedimentation has been added as was discussed in the reply to your number 3 major comments, see page 5 lines 15-22.**

14. P. 4, L. 24: the reference to Shaw (2003) is not correct here. The shear near cloud edges comes from cloud dynamics, not evaporation, see original study of Grabowski and Clark (1993) and more recent support from Park et al. (2017).

**The statement from Shaw (2003) has been removed from the manuscript. Turbulent kinetic energy is no longer discussed in the new manuscript.**

15. P. 5, L. 1: Should Twomey's or Squiers' old classical papers on droplet activation and growth be referred to here instead of Small and Rosenfeld?

**The statement in which this comment is referring to has been removed from the new manuscript. However, we have cited Twomey (1997) in relation to aerosols and cloud droplet size on page 13 lines 11-12 of the new manuscript.**

16. P. 5, L. 9: Rather than Pinsky and Khain, the original inhomogeneous mixing papers (John Latham, Marcia Baker, etc.) should be brought here.

**The statement in which this comment is referring to has been removed from the new manuscript. However, since we have shifted the focus to entrainment mixing, we do include multiple citations from Baker, including Baker et al. (1980) on page 2 line 24 and Baker et al. (1984) on page 2 line 32.**

17\*. P. 6, L. 23. Please explain how the normalization is done. Is the PCF simply shifted up or down to have zero at large scales? If this is an entrainment zone and droplets are clustered at large scales (as clearly illustrated in the left panel of Fig.1), the analysis should show that! This aspect is completely missed by the normalization. If the purpose of the analysis is to show small-scale clustering, then estimating the absolute magnitude of such small-scale clustering is impossible with the normalization.

**A detailed description of the normalization process has been provided in the reply to Major comment number 4. But in short, yes the PCF is simply shifted up or down to converge to a set value at larger values (in our case the set value is zero). Again, normalization is no longer done in the new manuscript.**

18\*. P. 7, L. 17. Fig. 1 clearly shows that the patchiness is at large scales (meters), not at small scales. Renormalization takes this aspect away. Is the focus of the analysis on concentration fluctuations at large scale (meters) or at small scales (centimeters) scale? I would think the latter. To me this is the key flaw of the analysis.

**We believe you are correct (along with Referee 2's comments) in stating that the PCFs in this paper should be more appropriately associated with the inhomogeneity occurring at larger scales due to the entrainment of dry air, as opposed to inertial clustering. An explanation of the PCF curve and how it should look for inhomogeneous data is given in the new manuscript on page 6 lines 13-21, and this is also conveyed on page 7 lines 9-12 in describing the PCF for real data calculated in Figure 1. It is believed that the PCF scale we currently use does not extend to small enough scales to even measure inertial clustering (we would need to measure down to mm, whereas we currently only extend down to ~ 3 cm). Lehmann et al. (2007) does not record an increase in the PCF due to inertial clustering for cumuli until length scales of approximately 1mm. We do not extend to the mm scale because we would need to reduce the dt used to calculate the PCF (see page 6 line 24-26), which would result in an even noisier PCF than what is already displayed.**

19\*. Fig. 5. First, I am curious how the figure looks without the normalization (see major point 3 above). The specific discussion in lines 15-20 on p. 9 may change if no normalization is performed. For instance, I think the statement on line 21 ("droplet spacing shifts from non-homogeneous to homogeneous at larger spatial scales") is incorrect as I expect the cloud edge to be quite heterogeneous at large scales (meters and up). The interpretation the authors provide comes from the normalization and it is counterintuitive.

**As can be seen in Figure 5 of the new manuscript, the overall PCF characteristics are unchanged. The main difference in the de-normalized curves is that they no longer converge to zero at the largest spatial lags on the x-axis (some PCF curves are greater than or less than zero). In relation to the discussion that was originally in lines 15-20 on page 9 (which can now be found on page 9 lines 16-22 in the new manuscript), you can see that the overall conclusions remain unchanged. L1, H1, and H2 still remain statistically significant from each other (when comparing center and edge data) while L2 is still statistically**

similar. In relation to the statement “droplet spacing shifts from non-homogeneous to homogenous at larger spatial scales”, this statement was made because we were forcing the PCF to zero (therefore, the statistical significance broke down at larger PCF values), not because homogenous conditions were physically present within the cloud at the time of measurement. Although this statement has been removed in the revised manuscript, this should have been made more clear originally.

20. Fig. 6. I do not understand what the value of the PCF is shown. Is that the asymptotic values at small scales (i.e., the left edge in Fig. 1)?

Yes, the PCF value is the average of the left-most edge of the PCF curve (the first 21 PCF values in the original manuscript). In the revised manuscript, the PCF value shown is an average of the first 60 PCF values that make up the x-axis. In other words, it is the average of the PCF values below ~ 1 meter (or the PCF values that make up the ‘shoulder’ region of the PCF curve).

#### References:

Baker, M., Corbin, R., and Latham, J.: The influence of entrainment on the evolution of cloud droplet spectra: I. A model of inhomogeneous mixing, *Quart. J. Roy. Meteor. Soc.*, **106**, 581-598, 1980.

Baker, M., Breidenthal, R., Choulaton, T., and Latham, J.: The effects of turbulent mixing in clouds, *J. Atmos. Sci.*, **41**, 209-304, 1984.

Good, G., Gerashchenko, S., and Warhaft, Z.: Intermittency and inertial particle entrainment at a turbulent interface: The effect of the large-scale eddies, *J. Fluid Mech.*, **694**, 371-398, 2012.

Ireland, P. and Collins, L.: Direct numerical simulation of inertial particle entrainment in a shearless mixing layer, *J. Fluid Mech.*, **704**, 301-332, 2012.

Lehmann, K., Siebert, H., Wendisch, M., and Shaw, R.A.: Evidence for inertial clustering in weakly turbulent clouds, *Tellus B*, **59**, 57-65, 2007.

Saw, E. Shaw, R., Salazar, J., and Collins, L.: Spatial clustering of polydisperse inertial particles in turbulence: II. Comparing simulation with experiment, *New Journal of Physics*, **14**, 105031, 2012.

## Reply to Comments made by RC 2.

Note that the reply is in bold.

**We would like to start by addressing concerns raised by both of the Referees. First, we apologize for the delayed response and posting of the revised manuscript. We put in a great deal of time and effort to do a rewrite of the paper, to shift the focus from the smaller scale clustering originally discussed to larger scale mixing as a result of entrainment. Both Referees raised concerns that the PCFs examined are more closely related to entrainment mixing as compared to preferential concentration, and we have also come to that conclusion. In particular, our PCF spatial scale does not extend into the Kolmogorov range, suggesting that inertial clustering (if present at all) isn't being measured. Our PCF curves also mirror those presented in Good et al. (2012) and Ireland and Collins (2012), which used the PCF for the purpose of analyzing larger-scale clustering due to entrainment mixing. Lastly, we have de-normalized all PCF curves displayed throughout the manuscript. In Saw et al. (2012) the PCF curves are normalized at the range the larger scale inhomogeneous mixing is occurring (i.e., the 'shoulder' region of the curve). Since the 'shoulder' region of the curve is what we are analyzing, normalizing it to a common value becomes unreasonable.**

The paper is on analysis of field experiment data pertaining to droplet clustering in clouds. This is an important subject considering that the experimental evidence for preferential concentration (inertial clustering) due to interaction with turbulence has been well established in the laboratory since at least a decade ago, yet it has never been satisfactorily documented from field data of atmospheric clouds (as far as I know). The main difficulty stems from statistical non-stationary commonly encountered in cloud data, as the author have discussed in the current manuscript.

The methodology and the foundation of such practice, the authors failed to disclose, has evolved and, in my view, sufficiently matured in the course of time since Shaw et al. (2002). A mathematical foundation (or origin) of the multiplicative effect of larger scale inhomogeneity on small scale clustering signatures in the Radial Distribution Function (by definition = PCF+1) was exposed (if not proved in strict mathematical sense) in Saw et al. (2012); the same paper also includes a demonstration, using experimental data, of how large scale inhomogeneity resulting from incomplete turbulent mixing caused an apparent uniform upward "shift" of the inertial clustering signatures at small scales. In short, it was shown that the mathematics of how RDF is calculated dictates that: when two concurrent phenomena of inhomogeneities are uncorrelated

and occurs with sufficient scale separation, the plainly calculated RDF equals the product of two RDFs, each results from the one of the two phenomena acting alone, i.e.  $g(r) = g_1(r) * g_2(r)$ .

**We do believe a better job could have been done in explaining the normalization process due to the confusion that has been shown. Although not discussed or included in the revised manuscript, originally we believe the process by which we did the normalization was flawed. In particular, we were normalizing the PCF curves at the largest scales where the PCF continues to decrease sharply (the region directly after the shoulder region) in order to analyze the differences in the shoulder region. However, in Saw et al. (2012) the PCF is normalized at the shoulder region in order to compare differences in the inertial clustering.**

**We are unaware of any work that has been conducted which shows PCF normalization is valid at the largest scales in order to analyze the shoulder region scale clustering. Although it has been shown that the PCF can be normalized in the shoulder region to analyze inertial clustering, normalizing the PCF at the largest scales to analyze the entrainment scale clustering may or may not be valid. Although this in and of itself could be an interesting project for future thought. Since we are no longer performing the normalization, we do not mention anything about this within the new manuscript.**

The above discussion, while relieving the doubts on the normalizing practice, unfortunately triggers another conundrum. Referring to the results (e.g. Figure 4) in Saw et al. (2012), the RDF signature associated with mixing of large (above Kolmogorov) scale inhomogeneity is a curve monotonic increasing with decreasing scale at first, transitioning into a plateau as we approach dissipative scales (the height of the plateau gives a relative measure of the level of inhomogeneity observed). The shape of the corresponding PCF would be qualitatively similar (but somewhat stretched at the large scale end) and this is remarkably similar to all of the PCF seen in the current paper. While, on the other hand, the RDF signature associated with inertial clustering, as found in many previous studies (many direct numerical simulation studies, theories and some experiments e.g. Saw et al. (2012)), have shapes suggestive of power-laws. Thus, it is reasonable to ask if the resulting PCFs in this paper should be more appropriately associated with the inhomogeneity at cloud edges due to entrainment and thus mixing dry and cloudy air, rather than with inertial clustering? Such a view is not inconsistent with the authors own estimate of Stokes numbers of the observed droplets, which is on the order of 0.01 (although we don't really

know how good is the  $100\text{cm}^2 \text{ s}^{-3}$  guess for the energy dissipation rate). Previous works suggests that  $\text{St Order}(0.01)$  should results in RDF with power-law exponent of order 0.01 or less, very likely indistinguishable from a plateau or flat horizontal line, given realistic signal-

noise ratio of in-situ cloud measurements.

**As already mentioned, we believe you are correct in stating that the PCFs in this paper should be more appropriately associated with the inhomogeneity at cloud edges due to entrainment and the subsequent mixing of dry and cloudy air, as opposed to inertial clustering. An explanation of the PCF curve and how it should look for inhomogeneous data (as you state above) is given in the new manuscript on page 6 lines 13-21, and this is also conveyed on page 7 lines 9-12 in describing the PCF for real data calculated in Figure 1.**

**We also agree that any inertial clustering that is present would be indistinguishable from the noise the current PCFs display. But it is believed that the PCF scale we currently use does not extend to small enough scales to even measure inertial clustering anyways (we would need to measure down to mm, whereas we currently only extend down to ~ 3 cm). Lehmann et al. (2007) does not record an increase in the PCF due to inertial clustering for cumuli until length scales of approximately 1mm. We do not extend to the mm scale because we would need to reduce the dt used to calculate the PCF (see page 6 line 24-26), which would result in an even noisier PCF than what is already displayed.**

I think major addition/revision is needed to convincingly disentangle mixing signatures from inertial clustering signature, otherwise the paper might have to be rewritten with a different focus (see below).

In relation to points above, perhaps I would suggest, if I might be so bold, that the current data might be better used for careful study of the RDF signatures of the cloud edge entrainment-mixing, which is perhaps also of interest? A good understanding of this will certainly be informative for discovery of proper methods of disentangling entrainment-mixing from inertial clustering in cloud data.

**As you have suggested, we have completely rewritten the paper to focus on clustering as a result of entrainment mixing as opposed to inertial clustering. We believe that focusing our results on entrainment provides a better analysis and explanation of the PCF signatures that are shown throughout the manuscript.**

**Although the most significant challenge in all field studies of clouds is distinguishing clustering due to droplet inertia from clustering due to entrainment and mixing (Lehmann et al. 2007), I don't believe the PCF curves displayed here would be appropriate for**

**disentangling entrainment-mixing from inertial clustering since our curves do not extend down into the Kolmogorov range. The fact that our curves don't include inertial clustering also makes them ideal for examining the clustering effect due to entrainment, since we don't have to worry about the Kolmogorov scale effects.**

minor comments: page 4, line 31: replace "by" with be page 8, line 1: time should have units in seconds not meter.

**The section of text that originally included page 4, line 31 has been removed. Units have been changed from meters to seconds (see page 7, line 31).**

**References:**

**Good, G., Gerashchenko, S., and Warhaft, Z.: Intermittency and inertial particle entrainment at a turbulent interface: The effect of the large-scale eddies, *J. Fluid Mech.*, 694, 371-398, 2012.**

**Ireland, P. and Collins, L.: Direct numerical simulation of inertial particle entrainment in a shearless mixing layer, *J. Fluid Mech.*, 704, 301-332, 2012.**

**Lehmann, K., Siebert, H., Wendisch, M., and Shaw, R.A.: Evidence for inertial clustering in weakly turbulent clouds, *Tellus B*, 59, 57-65, 2007.**

**Saw, E. Shaw, R., Salazar, J., and Collins, L.: Spatial clustering of polydisperse inertial particles in turbulence: II. Comparing simulation with experiment, *New Journal of Physics*, 14, 105031, 2012.**

## List of Major Changes

1. Figures 6 and 7 in the new manuscript have been added (they were not present in the original manuscript).
2. Panel (b) in Figure 8 (displaying median drop size) has been added (this panel was not represented in the original manuscript).
3. The first column in Table 1 from the original manuscript has been removed.
4. Table 8 from the original manuscript has been removed.
5. Section 5.3 in the original manuscript “Aerosol Number Concentration” has been removed. The information that was originally in Section 5.3 has been merged with Section 5.2 in the new manuscript.

Other things to note include:

- NONE of the PCF curves are normalized in the new manuscript.
- The new manuscript now focuses on larger scale clustering due to entrainment mixing, as compared to small scale inertial clustering in the original manuscript.
- **For the tracked changes below, added text is in blue, removed text is in red.**

# Droplet Clustering in Shallow Cumuli: The Effects of In-Cloud Location and Aerosol Number Concentration

Dillon S. Dodson.<sup>1</sup> and Jennifer Small Griswold<sup>1</sup>

<sup>1</sup>Department of Atmospheric Sciences, University of Hawaii, Manoa, Honolulu, HI, USA

**Correspondence:** Jennifer Small Griswold (smalljen@hawaii.edu)

**Abstract.** Aerosol–cloud interactions are complex, including albedo and lifetime effects that cause modifications to cloud characteristics. With most cloud–aerosol interactions focused on the previously stated phenomena, there has been no in-situ studies that focus explicitly on how aerosols can affect [large-scale droplet inhomogeneity](#) (droplet clustering) within clouds. This research therefore aims to gain a better understanding of how droplet clustering within cumulus clouds can be influenced by in-cloud droplet location (cloud edge vs. center) and the [surrounding environmental](#) aerosol number concentration. The pair-correlation function (PCF) is used to identify the magnitude of droplet clustering from data collected onboard the Center for interdisciplinary Remotely-Piloted Aircraft Studies (CIRPAS) Twin Otter aircraft, flown during the 2006 Gulf of Mexico Atmospheric Composition and Climate Study (GoMACCS). Time stamps (at  $10^{-4}$  m spatial resolution) of cloud droplet arrival times were measured by the Artium Flight Phase-Doppler Interferometer (PDI). Using four complete days of data with 81 non-precipitating cloud penetrations organized into two flights of low (L1, L2) and high (H1, H2) pollution data shows more clustering near cloud edge as compared to cloud center for all four cases. Low pollution clouds are shown to have enhanced overall clustering, with flight L2 being solely responsible for this enhanced clustering. Analysis suggests cloud age plays a larger role in the clustering amount experienced than the aerosol number concentration, with dissipating clouds showing increased clustering as compared to growing or mature clouds. Results using a single, vertically developed cumulus cloud demonstrate more clustering near cloud top as compared to cloud base.

## 1 Introduction

The spatial inhomogeneity of cloud droplets (i.e., droplet clustering) at different spatial scales has impacts on multiple cloud processes, including precipitation formation on the smallest scales (Kolmogorov scale, from here on termed *inertial clustering*) and radiative heating and cooling on the largest spatial scales. The work presented here deals with in-situ measurements of the magnitude of cloud droplet spatial inhomogeneities at scales of centimeters to tens of meters (from here on termed *droplet clustering* or just *clustering*) to provide information on how the entrainment mixing present at cloud–clear air interfaces impacts inertial particles (i.e. cloud droplets).

This information is of interest due to the complex physical processes controlling clouds, in particular the formation of precipitation and aerosol–cloud interactions, both of which can affect cloud lifetime and size. Along with these uncertainties, one of the main problems with cloud microphysical research has been determining how turbulence and mixing processes occurring

on smaller scales affect the macroscopic evolution of clouds (in particular the cloud droplet size distribution), along with gathering in-situ data to better understand these properties (Shaw, 2003; Grabowski and Wang, 2013). Due to the complexity of these processes, clouds are responsible for the greatest uncertainty when estimating climate sensitivity.

The physical processes controlling clouds are complex, with two of the largest uncertainties being precipitation formation and aerosol-cloud interactions, both of which can affect cloud lifetime and size. Along with these uncertainties, one of the main problems with cloud microphysical research has been determining the importance of turbulence on extremely small scales in affecting the macroscopic evolution of clouds, along with gathering in-situ data to better understand these properties (Shaw, 2003). These uncertainties and problems lead to clouds being one of the largest inaccuracies when estimating climate sensitivity.

Cloud droplets grow through the diffusion of water vapor up to sizes where collision-coalescence occurs. However, the rapid onset of rain (typically 15 to 20 minutes observed through radar measurements (Laird et al., 2000; Szumowski et al., 1997)) is difficult to explain using classical droplet growth theory. This is due to uniform condensational growth of cloud droplets leading to a narrowing of the drop size distribution, while most observed distributions are much broader. For example, the predicted growth time of precipitation calculated by Jonas (1996) of 80 minutes is four times slower than that observed. Although progress in modeling the formation of rain has been made (i.e., Wyszogrodzki et al. (2013); Seifert et al. (2010); vanZanten et al. (2011)), improvements still need to be implemented; in particular, in developing a better understanding of precipitating processes and the resulting feedbacks to implement better microphysical schemes (Wyszogrodzki et al., 2013). It has long been proposed that the entrainment of dry air into the cloud causes the broad size distributions observed (J. Warner, 1969; Telford and Chai, 1980; Jonas and Mason, 1982). Khain et al. (2000) states that the smallest droplets form through nucleation of drops during entrainment of drop-free air into the cloud, while the largest droplets are formed during inhomogeneous mixing leading to a local increase in the supersaturation.

Focusing on precipitation formation, there appears to be a factor of two or more difference between the predicted growth time of precipitation calculated by Jonas (1996) of 80 minutes and the observed growth time of 15 to 20 minutes from radar measurements made by Laird et al. (2000) and Szumowski et al. (1997), as discussed in Lehmann et al. (2009). Cloud droplets of radii less than 10 to 15  $\mu\text{m}$  grow efficiently through diffusion of water vapor while droplets larger than 30 to 50  $\mu\text{m}$  grow efficiently through gravitational collisions (Langmuir, 1948; Kogan, 1993; Pruppacher and Klett, 1997). In general, it is hard to explain the rapid growth of cloud droplets in the size range from 10 to 50  $\mu\text{m}$  (the so-called size gap), for which neither the condensation nor the gravitational collision-coalescence mechanism is effective. Multiple theories have been proposed to explain the short rain formation time observed, including: turbulent deviations in supersaturation (Vaillancourt et al., 2002); entrainment mixing (Khain et al., 2000; Lehmann et al., 2009); giant (GN) and ultragiant (UGN) nuclei (with diameters greater than 2  $\mu\text{m}$  and 10  $\mu\text{m}$ , respectively (Knight et al., 2002)); and the turbulent enhancement of collision-coalescence due to droplet clustering. Although each of these theories has merit, no one theory has been able to explain the fast formation of rain that is observed (i.e., Srivastava (1989); Vaillancourt et al. (2002); Rosenfeld et al. (2002); Feingold et al. (1999)).

Shifting our focus to aerosols, it is known that the effects of aerosols on clouds can lead to increased cloud lifetime due to the suppression of rain formation and to higher cloud albedo due to smaller droplets, better known as the cloud lifetime

and albedo effects, respectively (Small et al., 2009). Enhanced evaporation from smaller droplet sizes arises from aerosol perturbations, resulting in a stronger horizontal buoyancy gradient and increased entrainment, (known as the evaporation–entrainment feedback mechanism) as shown in both simulation (Xue and Feingold, 2006) and observational (Small et al., 2009) studies, where increased (decreased) entrainment could leads to decreased (increased) cloud lifetimes. This suggests  
5 that aerosol perturbations can lead to modifications of the turbulent environment within clouds, specifically at the entrainment interface , influencing the amount of dry air being entrained into the cloud. According to Ramaswamy et al. (2001), although increased aerosols are known to casue a negative forcing on the radiative budget when interacting with clouds, the magnitude of that negative forcing has the largest uncertainty as compared to other components considered (greenhouse gases, surface albedo, etc.) when studying factors contributing to cliamte change.

10 It is generally assumed that sub–saturated (droplet free and laminar) ambient air is entrained in ‘blobs’ due to the turbulent motions of the cloud. This results in a reduction in the total liquid water and directly influences the droplet size distribution. As suggested by Baker et al. (1980), the exact influence of entrainment mixing on the drop size distribution can be described by the Damkohler number (see Small et al. (2013)), which relates the time scales for turbulent mixing ( $\tau_{mix}$ ) and droplet evaporation( $\tau_{evap}$ ). Homogeneous mixing ( $\tau_{evap} \gg \tau_{mix}$ ) results in the drop size distribution shifting towards smaller diam-  
15 eters due to all droplets experiencing the same sub–saturation. Inhomogeneous mixing ( $\tau_{evap} \ll \tau_{mix}$ ) results in a decrease in the overall droplet number (while the drop size distribution remains unshifted) due to droplets experiencing different sub–saturated and super–saturated values.

After initial entrainment of the ambient, drop free air into the cloud, the subsequent turbulent mixing within the cloud acts to produce smaller and smaller parcels of sub–saturated cloudy and ambient air until the Kolmogorov length scale (approximately  
20 1 mm for atmospheric conditions, depending on the turbulent kinetic energy dissipation rate) is reached (Baker et al., 1984; Brenguier, 1993). Direct Numerical simulations (DNS) by Ireland and Collins (2012) and experimental results by Good et al. (2012) of particle entrainment showed droplet clustering resulting from the initial entrainment of particle free (non–turbulent) air into the particle laden turbulent air, with a decrease in the observed clustering in time due to turbulent mixing. Large scale spatial inhomogeneities resulting from mixing have also been observed and discussed by Saw et al. (2008) and Saw et al.  
25 (2012).

The complexity of clouds can clearly be seen from the discussion above, and a better understanding of said complexity can be gained by understanding droplet clustering on the smallest scales. Up until the late 1980’s, it was mostly accepted that droplet spacing within clouds was statistically homogeneous, or uniformly distributed according to Poisson statistics (Marshak et al., 2005; Rogers and Yau, 1989). Srivastava (1989) argued that in most numerical studies of cloud physics it is assumed that droplet  
30 to droplet variability is not important in calculating the growth of an ensemble of droplets. However, this conclusion must be viewed as tentative due to evidence that has been gathered over the past three decades for the inhomogeneous distription of droplet populations at all length scales droplet clustering occurring specifically at the millimeter and centimeter scales (e.g., Baker (1992); Kostinski and Jameson (1997); Kostinski and Shaw (2001); Larsen (2007); Siebert et al. (2010); Shaw et al. (1998, 2002)). The presumption that droplet spacing is homogeneous has consequences for cloud parameterizations in  
35 microphysical models such as the formation of precipitation. For example, the stochastic collection equation, used to describe

the growth of droplets via collision–coalescence, assumes that droplets are homogeneously distributed and not preferentially concentrated (Kostinski and Shaw, 2001). An enhanced collision kernel and collision efficiency also results from droplet clustering (Pinsky et al., 1999; Grabowski and Wang, 2013). Quantitative results from Pinsky et al. (2008) found that droplet growth can be enhanced by a factor of 2–3 through turbulent collision–coalescence, while Grabowski and Wang (2009) found that growth was enhanced between factors of 1.2 to 4.5 based on different values of turbulent kinetic energy (TKE) dissipation rates.

Analysis of droplet observations in adiabatic cores of cumulus clouds from Chaumat and Brenguier (2001) display droplets that are randomly distributed (homogeneous) on the small and large scales, albeit, this homogeneous droplet distribution is observed in adiabatic cores away from dry air entrainment at cloud edge. These results are in disagreement with the aforementioned studies in the previous paragraph, suggesting more in–situ studies into droplet clustering need to be performed. The in–situ observations of droplet spatial distributions that do exist are scarce, with most studies (i.e., Shaw et al. (2002); Lehmann et al. (2007)) focusing on single cloud traverses and/or quantifying the statistical tools used to measure said clustering. Our understanding of the motion of inertial particles in turbulence has advanced considerably, particularly due to the study of inertial clustering at the Kolmogorov scales (i.e., Maxey (1987); Squires and Eaton (1991); Shaw et al. (1998); Eaton and Fessler (1994); Sundaram and Collins (1997)). However, this understanding has not been extended to particles being clustered due to larger scale influences such as the entrainment mixing found at the boundaries of clouds. The work conducted here therefore becomes important due to the fact that a dataset is provided that gives in–situ cloud droplet spatial data allowing for an investigation into the influence that entrainment has on droplet clustering.

One of the main difficulties in turbulence and droplet clustering work as explained by Pinsky et al. (2006) is no measurements of the fine turbulent structure in clouds have been carried out. Most laboratory experiments are conducted for Reynolds number values that are much smaller than those typically found for atmospheric turbulence. Since the structure of a turbulent flow depends on the Reynolds number, it is not clear how the results obtained in laboratory experiments can be extended to atmospheric conditions. The work conducted here therefore becomes important due to the fact that a dataset is provided that gives in–situ cloud droplet spatial data that allows for an analysis of spatial variability, and the fact that droplet spatial variations can be compared to laboratory measurements to see if they can indeed be extended to atmospheric conditions.

This research focuses on the fundamental investigation of droplet clustering, specifically how it changes within clouds (cloud edge vs. cloud center, as a function of cloud height) and different cloud environments (low vs. high pollution clouds). Specific questions in regards to droplet clustering in shallow, warm continental cumulus clouds to be answered include: (1) Does droplet clustering change as a function of location (cloud center vs. edge)? It is hypothesized that clustering will be enhanced at cloud edge where entrainment of dry air is directly occurring. Turbulent mixing will reduce the large scale inhomogeneities in the droplet population moving towards cloud center. (2) Does droplet clustering change as a function of cloud height? It is hypothesized that an increase in clustering will be present near cloud top due to the entrainment of dry air. (3) Does droplet clustering depend on aerosol number concentration? It is hypothesized that an increased aerosol load leads to enhanced clustering due to the resulting increased entrainment from smaller droplet sizes and evaporation. This information can eventually be used to develop better cloud microphysical parameterizations not only for modeling precipitation, but for modeling the overall role

of clouds in radiation models. Section 2 will introduce droplet clustering and the statistical tool used to measure the clustering. Section 3 will discuss data collection and instrumentation along with environmental and flight characteristics. Section 4 will provide results related to the three scientific questions proposed above. Section 5 will lead to a discussion of the results, including a hypothesis on how clustering is influenced by cloud age, followed by concluding remarks.

5 This is a first step in developing a better understanding of droplet clustering as a result of entrainment mixing, in the hopes of eventually leading to better cloud microphysical parameterizations for modeling precipitation and the overall role of clouds in radiation models. Section 2 will provide a deeper introduction into droplet clustering along with the pair-correlation function (the statistical tool used to measure the clustering). Section 3 will discuss data collection and instrumentation along with environmental and flight characteristics. Results related to the three scientific questions proposed above are presented in Section  
10 4. Finally, in Section 5 we discuss and summarize the work presented and provide suggestions for extending the analysis presented here.

## 2 Droplet Clustering and the Pair–Correlation Function (PCF)

### 2.1 Droplet Clustering

As briefly introduced in Section 1, droplet inhomogeneity inherently occurs on different spatial scales. It has been proposed  
15 in multiple studies (i.e., Shaw et al. (1998); Eaton and Fessler (1994); Sundaram and Collins (1997)) that **droplet clustering** inertial clustering **also known as preferential concentration or inertial clustering** can be understood as the result of particles being centrifuged out of regions of high fluid vorticity (where vorticity is a measure of local rotation in a fluid flow) and thus preferentially concentrating into regions of high strain or low fluid vorticity as a consequence of their inertia. Sundaram and Collins (1997) have shown that the scale most responsible for preferential concentration is the Kolmogorov scale. This  
20 is partially supported by the fact that vorticity plays a key role in concentrating particles, and vorticity is predominantly concentrated in the smallest eddies (Tennekes and Lumley, 1972). **This is due to turbulence being dissipative. The dissipation of energy is most effective at small scales, which together with the fact that energy is mainly provided at large scales implies that energy is transferred from larger to smaller scales (energy cascade). Fluid inertia dominates over viscosity at larger spatial scales, while viscosity dominates at smaller scales (dissipation range). Preferential concentration is enhanced between the**  
25 **dissipation and inertial ranges because it is at these scales that turbulent vorticity is dominant (Wang and Maxey, 1993). Dissipative structures that appear within turbulence can be referred to as vortex tubes that infuse isotropic turbulence, where turbulence is said to be isotropic if rotation and buoyancy are not important and can be neglected, and there is no mean flow. Vortex tubes are relevant to the present discussion because they are thought to be responsible for ejecting particles into high strain regions of the flow (Shaw et al., 1998).**

30 The mechanism responsible for inertial clustering is completely unrelated to clustering that results from entrainment mixing, which is the focus of the work presented here. Inhomogeneous mixing (i.e., entrainment mixing) leads to the mixing of particles from one region of the flow to another on a spatial scale comparable to the length scale of the mixing eddies. The largest eddies are slightly smaller than the length scale of the cloud itself (Grabowski and Clark, 1993), while the smallest

mixing eddies are on centimeter scales. These mixing length scales have been observed in non-precipitating continental cumulus, with observations of the largest mixed cloud and clear air parcels on the scale of meters to tens of meters (Paluch and Baumgardner, 1989), with the smallest parcels down to centimeter scales from turbulent mixing of the larger parcels. Other observations (Baker, 1992; Brenguier, 1993) suggest sharp interfaces between mixed parcels down to centimeter scales, with Brenguier (1993) observing a change from near 0 to 2000 drops per cubic centimeter over a length scale of approximately 5 mm. These observations support the conceptual ideas of entrainment mixing, with the initial engulfment of ambient air followed by turbulent mixing of cloudy air down to the smallest scales.

Entrainment is found to be governed by the large-scale parameters of the flow. Veeravalli and Warhaft (1989) and Kang and Meneveau (2008) show that the entrainment interface is characteristic of turbulent bursts penetrating the low-turbulent region, resulting in non-turbulent (drop free) air being entrained into the turbulent region. The non-turbulent air then becomes turbulent through the viscous diffusion of vorticity at the interface. The viscous diffusion of vorticity is a Kolmogorov length scale process, while the entrainment rate at large Reynolds numbers is known to be independent of viscosity. This suggests that although the transition from non-turbulent to turbulent occurs through small eddies, its rate is governed by the larger eddies (Hunt et al., 2006). This suggests that the rate of entrainment determines the amount of droplet clustering present, with more entrainment leading to a larger droplet inhomogeneity due to larger and more numerous packets of environmental air being mixed with the cloud.

The particle response time ( $\tau_d$ ) is not the only value that determines whether or not particles will tend to cluster. The ratio of  $\tau_d$  to the relevant timescale of fluid accelerations is also of importance. Since clustering is associated with vorticity, and the vorticity spectrum peaks at small scales, the Kolmogorov timescale  $\tau_k$  is the relevant fluid time scale, where Saw et al. (2008); Hogan and Cuzzi (2001); Wood et al. (2005) have shown that inertial clustering is very sensitive to the particle Stokes number, given by:

$$S_t = \frac{\tau_d}{\tau_K} = \frac{\rho_w d^2 \varepsilon^{\frac{1}{2}}}{18 \rho_a \nu^{\frac{3}{2}}} \quad (1)$$

is the Stokes number (Vaillancourt et al., 2002), with where  $\rho_a$  and  $\rho_w$  representing the density of air and liquid droplets, respectively,  $d$  the droplet diameter,  $\nu$  the fluid kinematic viscosity, and  $\varepsilon$  the turbulent energy dissipation rate,  $\tau_d$  the particle response time, and  $\tau_K$  the Kolmogorov timescale. The Stokes number characterizes a particles inertial response to the flow. Particles with  $St \gg 1$  react very slowly to changes in the flow, while particles with  $St \ll 1$  follow the flow exactly. For the range of Stokes number in clouds ( $St \ll 1$  to  $St < 1$ ), inertial clustering increases as the droplet size increases or as the turbulent dissipation rate increases, with inertial clustering peaking at  $St \sim 1$  and decreasing for smaller Stokes values. Droplet clustering is related to  $S_t$  by the power law:

$$\eta(r) \propto \left(\frac{r}{r_K}\right)^{-f(S_t)} \quad (2)$$

where  $\eta(r)$  is the spatial pair-correlation function (used to measure the amount of clustering, see Section 2.2),  $r_K$  is the Kolmogorov length scale, and  $f(S_t) > 0$  increases monotonically with  $S_t$  for  $S_t < 1$  (Saw et al., 2008). This implies that clustering increases for increasing  $S_t$  (for values between zero and one). Hogan and Cuzzi (2001) and Wood et al. (2005)

also concluded that clustering is at a maximum for Stokes numbers near one. This suggests that clustering depends on the droplet size and the turbulent dissipation rate. It is known that the typical range of Stokes number in clouds is  $S_t \ll 1$  to  $S_t < 1$  (Vaillancourt et al., 2002; Fouxon et al., 2015; Moghadaripour et al., 2017), indicating that for the range of Stokes numbers that occur in clouds, clustering increases as the droplet size increases or as the turbulent dissipation rate increases.

5 It is important to note that how droplet clustering is related to turbulence will be discussed, but no actual turbulence parameters will be measured due to data availability, leaving for the chance of future work to expand on the results presented here. For example, one would expect that turbulence should be enhanced near cloud top and edge where the entrainment of non-turbulent air is mixed with turbulent cloudy air (Siebert et al., 2006). Shaw (2003) also states that one of the main sources of TKE in clouds is shear evaporative cooling due to the entrainment of dry air at cloud edge and top. Direct measurements  
10 have shown that the mean TKE dissipation rate peaks near cloud top at its edge (MacPherson and Isaac, 1977; Gerber et al., 2008). It can therefore be hypothesized that droplet clustering will be enhanced at cloud edge (top) as compared to cloud center (bottom) due to increased Stokes numbers. On the contrary, an increase in aerosol number concentration will lead to a decrease in droplet size (Small et al., 2009; Rosenfeld et al., 2008), a decrease in the Stokes number, and a decrease in droplet clustering. Note that while clustering may well be enhanced at cloud edge or top, the reason for this enhanced clustering is made based on  
15 previous work and is speculative due to the fact that TKE is not directly measured here. This work sets out to simply determine how the spatial variability of droplet clustering changes with in-cloud location and aerosol number concentration, leaving the direct relationship between in-cloud turbulence and clustering for future work.

It is important to state that preferential concentration and the physical processes leading to it at the millimeter and centimeter scales is different than the inhomogeneity in droplet concentration that occurs at larger scales on the order of several meters.  
20 Larger scale inhomogeneity is caused by the inhomogeneity of turbulence (fluctuations of vertical velocity) and cloud condensation nuclei (Pinsky and Khain, 2002, 2003), and the entrainment of sub-saturated air containing few or no droplets (Krueger et al., 1997). The inhomogeneity of the droplet population at larger scales will be accounted for, as will be discussed in Section 2.3.

However, Good et al. (2012) and Ireland and Collins (2012) have shown that mixing-driven droplet clustering is only weakly  
25 dependent on the particle Stokes number. Unlike inertial clustering, large scale droplet clustering due to entrainment should exist even as the Stokes number approaches zero. Droplet clustering would only be reduced as the Stokes number approaches infinity (such as heavy particles) due to the droplets not following the turbulent flow as dry air is entrained.

The effect that gravity (i.e., droplet sedimentation) has on the droplet response to the fluid must also be considered. Grabowski and Vaillancourt (1999) suggest if the droplet terminal velocity is much larger than the Kolmogorov velocity scale,  
30 then the particle will fall through the microscale structures associated with the turbulent flow regardless of the particle inertia. Ireland and Collins (2012) found that particles are less dependent on the turbulent fluctuation for enhanced gravity, leading to lower levels of droplet clustering as compared to the reduced gravity case. Ireland and Collins (2012) also found enhanced settling of droplets with moderate Stokes numbers (larger droplet size), consistent with the findings in Wang and Maxey (1993) where droplets tended to cluster at the edges of vortical eddies leading to a preferential sweeping of the particles in a downward  
35 moving fluid. On the other hand, Good et al. (2012) observed reduced settling for droplets with moderate Stokes numbers. This

contradiction suggests more research into droplet spatial tendencies is needed. It is also important to note that the studies just discussed present results for Reynolds numbers that are smaller than those encountered in atmospheric clouds. Although the Reynolds number is shown to have a very weak dependence (if any at all) on droplet clustering, the results presented here can be used to compare in-cloud clustering measurements with clustering measurements from laboratory experiments made by

5 Ireland and Collins (2012) and Good et al. (2012).

## 2.2 Pair-Correlation Function

There are multiple tools that can be used to measure droplet clustering using a time series of droplet detection times, but the 1-D temporal pair-correlation function (PCF) will be used throughout this paper due to the advantages of the PCF outlined in Shaw et al. (2002); Shaw (2003); Larsen (2007, 2012); Baker and Lawson (2010). The PCF can be introduced as a scale-localized

15 deviation from a stationary Poisson distribution, where the PCF is given by:

$$\eta(t) = \frac{p(t_o + t|t_o)}{\lambda} - 1 \quad (3)$$

from Larsen (2012), where  $\eta(t)$  is the PCF,  $p(t_o + t|t_o)$  represents: given a particle detected at some time  $t_o$ , what is the probability of finding another particle in the time lag  $t_o + t$ . The mean number of droplets per time bin is given by  $\lambda$ . Calculating  $p(t_o + t|t_o)$  can become simplified by using:

$$15 \quad \eta(t) = -1 + \frac{1}{\lambda} \sum_{k=1}^{\infty} f_k(t) \quad (4)$$

where  $f_k(t)$  is the probability distribution function that the  $k^{th}$  particle posterior to a particle at  $t_o$  (the  $k^{th}$  nearest neighbor) is located at  $t_o + t$ , where it is assumed that co-located particles are impossible. Each of the  $f_k(t)$  can be estimated from the observed inter-arrival distributions (time between droplet arrival), thus allowing a computationally simple way to compute the PCF from particle arrival times **For more information and a derivation of the  $k^{th}$  nearest-neighbor function see** (Picinbono and

20 Bendjaballah, 2005; Larsen, 2007, 2012).

The main advantage of the PCF is the fact that it is scale localized. The PCF depends only on the presence or absence of particles separated by  $t$  in time (Larsen, 2012). Physically, when  $\eta(t) > 0$  there is an enhanced probability of finding a particle in the time frame  $t$ . The range of the PCF is  $(-1, \infty)$  with  $\eta(t) = 0$  representing perfect randomness and  $\eta(t) = 3$ , for example, resulting in a factor of 4 enhancement of finding another droplet time  $t$  away, as discussed in Kostinski and Shaw (2001).

25 **When measuring data that is non-stationary (i.e., large scale spatial inhomogeneities are present), the PCF is affected by clustering due to inertial and entrainment mixing affects** (Saw et al., 2008, 2012). This results in a PCF (see Figure 4 in Saw et al. (2012)) with a power-law-like region at the smallest scales (Kolmogorov scales) due to inertial clustering, followed by an extended ‘shoulder’ region due to entrainment mixing at larger scales (above Kolmogorov to tens of meters), followed by a rapid drop-off at even larger scales. Figure 3 in Shaw et al. (2002) demonstrates two PCF plots, one with data from an entire  
30 cloud penetration and another with only cloud center data. The PCF for the entire cloud traverse is shown to be shifted to larger clustering values due to large scale droplet concentration fluctuations caused by ‘holes’ in the cloud. Although Shaw et al.

(2002) does not elaborate on the cause of these cloud ‘holes’, for our purposes we can think of them as areas of decreased droplet concentration due to the entrainment of dry environmental air into the cloud.

Although the PCF is a great statistical tool for detecting droplet clustering, its physical sense is not so profound. Along with that, particle positions have been determined in 1–D space, although 3–D space would provide more information on the overall local concentration enhancement. Both issues can be accounted for from Holtzer and Collins (1997); Sundaram and Collins (1997) and Zhou et al. (2001). It should also be noted that the PCF is referred to as the radial distribution function ( $g(r) = \eta(r) + 1$ , where  $r$  represents distance as compared to time) in these papers (Shaw, 2003). Sundaram and Collins (1997) showed that preferential concentration can be accounted for in the Saffman–Turner collision kernel (Saffman and Turner, 1956) by a factor equal to  $\eta(t) + 1$ . This has been shown to be true for both monodisperse ( $g_{11}(r)$ ) and bidisperse ( $g_{12}(r)$ ) systems (Zhou et al., 2001), where  $g_{11}(r)$  and  $g_{12}(r)$  represents the radial distribution function (RDF) for each system, respectively. The droplets in this paper would be considered bidisperse as droplets of different sizes were used to calculate the PCF. To infer information about 3–D clustering, it has been shown in Holtzer and Collins (1997) that the 1–D PCF is equivalent to integrals of the 3–D PCF (Equation 2.5 from Holtzer and Collins (1997)). Although measuring the actual physical impact that the PCF has on collision–coalescence is beyond the scope of this paper, it is important to understand how the results obtained here can be used to better understand the physical processes that occur within clouds.

### 2.3 Calculating the PCF

The PCF is reliant on the fact that the underlying dataset must be statistically stationary/homogeneous (the mean and variance of the number of counts are assumed to be constant over the analyzed time interval). This is due to the fact that the PCF may deviate from zero not from a statistical correlation of clustering at smaller scales, but from inhomogeneity at larger scales (Larsen (2012) Appendix B). This requirement can be met when sampling horizontally homogeneous clouds such as stratus. For more turbulent cumulus clouds where stronger entrainment and mixing processes occur, this condition is usually only fulfilled for subsections of the cloud.

The PCF was calculated three times for each cloud penetration (120 m section, representing roughly 2 seconds worth of data) at cloud edge (cloud entry and exit) and cloud center. One-hundred and twenty meters represents a two second interval of data, which provided enough cloud droplets to run the PCF while not completely ignoring data stationarity. However, due to the data being slightly non–stationary nonetheless, each PCF calculation was normalized so it decayed to zero. The justification for PCF normalization comes from Shaw et al. (2002), where it was shown that the PCF shape is similar when comparing the PCF of an entire cloud penetration vs. just cloud center. The two PCF curves were separated by a vertical shift due to droplet concentration fluctuations occurring on scales larger than  $t$  from non–stationarity. Qualitatively however, the curves were identical. The small–scale clustering was shown to not be influenced by large scale fluctuations, making normalization possible (see Figure 3 in Shaw et al. (2002) for more information). Note that the PCF is a useful quantitative and qualitative tool, but anything quantitative must be carefully evaluated if it comes from data that is either nonstationary or not known to be stationary, again, stating the importance that this paper is only looking at how clustering changes with cloud location and with aerosol number concentration, and not drawing any quantitative results from the clustering on processes such as collision–

**coalescence.** To calculate the  $k^{th}$  nearest neighbor, a maximum time interval ( $t_{max}$ ) and time bin ( $dt$ ) are selected. Careful consideration must be given. Set  $dt$  too small, the PCF will be too noisy. Set  $dt$  too large, you end up doing unnecessary scale averaging which results in a poor estimate of the PCF. Typically,  $t_{max}$  is an order of magnitude or so above the mean inter-arrival time (MIT, mean time between each droplet within the data) of the particles and sets the maximum temporal lag.

5 A  $dt$  of 0.0003 seconds and a  $t_{max}$  of 0.2 seconds were selected for all PCF calculations throughout this paper. This results in a vector ranging from 0.000 to 0.2 by 0.0003, giving the temporal lag ( $x$ -axis) for each PCF measurement. **This results in a spatial range of  $\sim 3$  cm to 12 m, ideal for analyzing droplet clustering due to entrainment mixing.**

The PCF is calculated by binning the inter-arrival times of the droplets into the vector sequence seen above. An inter-arrival time is first determined between every subsequent droplet, binned and summed (the sum of each inter-arrival time per bin).

10 An inter-arrival time is then determined for every other droplet, every third droplet, every fourth droplet, and so on. The inter-arrival times are binned and added to the previously summed binned inter-arrival times up until the minimum inter-arrival time in the data is no longer less than  $t_{max}$ . The total summed binned data is then used to calculate the PCF from Equation 4.

Figure 1 gives a visualization and description of the PCF clustering signature, giving both temporal and spatial lag on the  $x$ -axis. Note that the PCF results presented from this point on will be in spatial lag (where spatial lag was estimated using the mean aircraft velocity) for the simplicity of being able to more easily comprehend spatial lag over temporal lag. The real data (top left) shows a peak at smaller spatial scales and a **steady** decrease to zero at larger spatial scales (**where the decrease starts at  $\sim 1.2$  m**) while the Poisson data (top right) shows the PCF varying around zero, indicating no clustering at any scale. **The mean of the two PCFs are 0.057 and  $1.94 \cdot 10^{-5}$  for the real and simulated data, respectively. The mean was calculated by taking the first 8 PCF values (covering a spatial scale up to 13 cm), since it is at smaller spatial scales in terms of analyzing droplet**

15 **clustering that we are concerned with. This displays that real cloud droplets have a greater amount of clustering as compared to droplets that have a perfectly random orientation. From a visual examination of the raw droplets (bottom panels), the real data is preferentially concentrated or patchy, whereas the Poisson point data is perfectly homogeneous. The PCF signature for the real data is indicative of droplet inhomogeneity at larger scales, where the 'shoulder' region of the curve is present before a decrease to zero (note that inertial clustering is not presented since the curve does not extend into the Kolmogorov length scale).**

20 **In comparing the two PCF curves, it is clear that real cloud droplets have a greater amount of clustering as compared to droplets that have a perfectly random orientation. A better visual representation of the droplet clustering that the PCF is displaying can be gained by analyzing the raw droplets (bottom panels), where the real data is patch or clustered and the Poisson point data is perfectly homogeneous.**

### 3 Data Collection and Characteristics

30 The Gulf of Mexico Atmospheric Composition and Climate Study (GoMACCS) was conducted jointly with the 2006 Texas Air Quality Study (TexAQS) during August and September of 2006 as a combined climate change and air quality intensive field campaign. The Center for Interdisciplinary Remotely-Piloted Aircraft Studies (CIRPAS) Twin Otter (flight speed of about 60  $m s^{-1}$ ) performed 22 research flights to explore aerosol-cloud relationships over the Houston and northwestern Gulf of Mexico

regions (Lu et al., 2008). Among the 22 research flights, 14 intensive cloud measurements were carried out (where the clouds were all continental warm cumulus subjected to various levels of anthropogenic influence), including one flight in which an isolated cumulus cloud of sufficient size and lifetime existed to allow detailed sampling at different altitudes. The other 13 cases involved scattered cumuli that were sampled in such a manner as to provide statistical properties over the cloud field (Lu et al., 2008), with each cloud being traversed through once, with and no one cloud being measured multiple times.

Table 1 shows each flight conducted during GoMACCS, with the corresponding Research Flight (RF) number, date, number of clouds in the flight after filtering (including clouds that are only  $> 300$  m in length and non-precipitating), the aerosol number concentration ( $N_a$ , measured by the condensation particle counter (CPC)), and the aerosol number concentration for accumulation mode particles ( $N_{acc}$ , measured by the passive cavity aerosol spectrometer probe (PCASP)), which includes aerosols that are only in the size range of  $0.1 \mu\text{m} < \text{particle size} < 2.5 \mu\text{m}$ . The Phase-Doppler interferometer (PDI, see Chuang et al. (2008)) was used to collect droplet velocity, size, and measurement time. It was found that the droplet arrival time can accurately be measured to  $< 3.5 \mu\text{s}$  from Saw (2008), resulting in accurately mapping droplets down to  $2.1 \cdot 10^{-4}$  m (assuming average aircraft speed). Note that there is no dead time in PDI measurements. For more information on each of the flights and the instrument payload, see Lu et al. (2008).

Following the methods in Small et al. (2013), two low (L1, and L2, where L1 (L2) is given by RF 5 (RF 22)) and high (H1, and H2, where H1 (H2) is given by RF 12 (RF 18)) pollution flights were selected out of the 22 research flights that occurred. The two least and most polluted flights were selected which had satisfactory cloud sampling for analysis of how aerosol number concentration effects droplet clustering. A Case Flight (RF 18 Flight 16) was selected where an isolated cumulus cloud was sampled at different altitudes for analysis of droplet clustering as a function of cloud height. Table 2 shows variables highlighting different cloud and environmental conditions within each flight. Note that the environmental lapse rate and relative humidity (RH) in Table 2 was calculated from data collected from out of cloud spirals, where the average RH was computed for the vertical range of cloud measurements for the respected flight. Table 3 gives a summary of average values for low and high pollution cases for select properties from Table 2.

Figures 2 and 3 show the flight altitude as a function of time with droplet counts per second overlaid (top panels) and the flight paths (bottom panels) for low and high polluted clouds, respectively. Note that the flight path for the Case Flight is not shown here. The average droplet counts (clouds) encountered per second (flight) for L1 and L2 were 660 (18) and 1016 (13), respectively. Whereas for H1 and H2, the average counts (clouds) encountered per second (flight) were 958 (29) and 3300 (21), respectively. Low pollution clouds were sampled to the North of Houston (upwind) and high pollution clouds were sampled to the Southwest (H1) and West (H2) of Houston (downwind), as confirmed using archived wind data from the NOAA National Center for Environmental Information and HYSPLIT trajectories (not shown here) from the Air Resources Laboratory (Stein et al., 2015).

It can be calculated from analyzing Table 3 that the high pollution clouds had roughly 2.5 times more aerosols per cubic centimeter than the low pollution clouds. The difference in aerosol number concentration between the low and high pollution clouds produce clouds that are statistically different from one another. Figure 4 shows cloud droplet diameter in microns ( $\mu\text{m}$ ) on the x-axis with aerosol number concentration ( $\text{cm}^{-3}$ ) on the y-axis, with low pollution data in green and high pollution data

in gold. Density curves are given to show how the data is distributed for the respected axis. The p-value (used to determine statistical significance between two datasets, where  $p\text{-value} < 0.05$  is considered significant, see Wilks (2011)) between low and high pollution cloud droplet size is  $3.99 \cdot 10^{-10}$  (average droplet diameter is  $13.4 \mu\text{m}$  ( $10.7 \mu\text{m}$ ) for low (high) pollution clouds). The linear best fit trend lines show that droplet size decreases with increasing aerosol number concentration, with R-squared values (the proportion of the variance in droplet size that is predictable from the aerosol number concentration) of 0.24 and 0.07 for low and high pollution, respectively. The p-value for the aerosol number concentration is  $< 2.22 \cdot 10^{-16}$ . Both properties of the droplet population have p-values less than 0.05, making the difference in droplet size and aerosol number concentration significant for the two populations of data. Having two statistically different data populations is ideal for comparing PCF values for low and high pollution clouds. If clustering does not change between the two, then an argument cannot be made for the statistical similarities in the data sets as a possible reason. Note that all p-values in this paper were calculated using the Wilcoxon-rank-sum-test, which is used to determine a statistical difference in the medians of two datasets that have different populations (Wilks (2011)).

## 4 Results

### 4.1 Edge, Center, and Cloud Top Clustering

PCF functions for L1, L2, H1, and H2 are given in Figure 5, moving from top left to bottom right, respectively, with blue (red) representing entrainment zone (cloud center) data. The two envelopes represent the 85<sup>th</sup> and 15<sup>th</sup> percent quantile of the data. The center lines in each envelope represent the entrainment edge and center mean clustering, with bold mean lines representing data that is statistically significant (p-value less than 0.05) and thin mean lines representing data that is statistically similar. The PCF functions for both center and entrainment zone data indicate clustering associated with larger-scale inhomogeneity, with the 'shoulder' region of the curves present out to  $\sim 1.2$  m, before a decrease to zero at spatial scales beyond  $\sim 1.2$  m. is at a maximum for lower spatial scales ( $< 30$  cm) and decreases towards zero at larger spatial scales for all four flights.

The main takeaway from Figure 5 is the larger degree of more dominant clustering signature at smaller spatial scales and the enhanced clustering for the entrainment for cloud edge as compared to the center zones for all four flights. Mean PCF and quantile values for edge and center data can be found in Table 4. The mean and quantile values were calculated by taking the first 60 PCF values (covering a spatial scale up to  $\sim 1$  m), since it is the 'shoulder' region of the PCF curve that we are interested in analyzing. The percent of statistically significant data (for the first 6021 PCF values, spatial lag  $\leq 1 \text{ m} \leq 36 \text{ cm}$ ) and the corresponding p-values can be found in Table 5. Note to calculate the p-value, every PCF curve generated for the respective plot was grouped. A p-value was then generated for each spatial-lag on the x-axis by calculating the Wilcoxon-rank-sum-test between the two sets of data for the specific x-axis location.

From analyzing Figure 5 and the corresponding tables, L1, H1 and H2 show clustering characteristics which are comparable to one another, including: (1) the mean PCF value for the edge entrainment data is always greater than the mean PCF value for the center data. (2) The 15<sup>th</sup> percent quantile value for the center data is always smaller than the 15<sup>th</sup> percent quantile value for the edge data. (3) The 85<sup>th</sup> percent quantile value for the edge entrainment data is always larger than the 85<sup>th</sup> percent

quantile value for the center data. (4) There is a statistical significance between the clustering occurring between the edge and center zones of the clouds. Note that the statistical significance in the clustering between the two zones breaks down at larger spatial scales (this is very apparent in the H1 case) as the PCF decays towards zero for both entrainment and center data. This is expected, since the two datasets converge to zero as the clustering disappears and droplet spacing shifts from non-homogeneous to homogeneous at larger spatial scales. (5) The mean PCF values for entrainment data are very similar, ranging from 0.50 to 0.54, whereas the range for the center data is between 0.18 to 0.30 (Table 4).

From analyzing L2 (bottom left panel) and the corresponding tables, there are significant differences from the other 3 cases. Although the mean edge clustering is enhanced as compared to the center zone, the difference is not statistically significant, with zero percent of the data having a p-value below 0.05 (average p-value of 0.400.30).

Another difference is the range of the quantile values, with the cloud edge entrainment data having a lower 15<sup>th</sup> percent quantile value than that of the center data, in contrast to what is observed in L1, H1, and H2. Another difference is the range of the 85<sup>th</sup> percent quantiles, with the two quantile values being virtually similar at 1.79 and 1.81 for center and entrainment zone data, respectively. Note that the mean clustering amount for L2 (both center and edge entrainment) is enhanced as compared to the other three cases (Table 4).

It is clear that there is enhanced clustering in the edge entrainment zone as compared to the center zone, but one needs to understand how to define if the overall clustering (both edge entrainment and center) is significant as compared to a randomly distributed droplet population. This is done by analyzing the range that the PCF can take on due to the random nature of the data. If the physical clustering measured falls outside of this range, then the conclusion can be made that the clustering being viewed is indeed real and not perfectly homogeneous. This test was performed on each of the four cases, following the methods outlined in Larsen and Kostinski (2005). For the data, 1000 Poisson simulations were produced (as is seen in the top right of Figure 1, showing a single Poisson simulation) using the same time duration and droplet count as the original data. These Poisson simulations then form an envelope of PCF values (using the maximum and minimum values from the 1000 simulations) one would consider homogeneous. PCF values that lie within the Poissonian simulation envelope were recorded by using the average PCF value and were labeled non-significant. Table 6 shows the percentage of PCF values for each flight, and each location (edge entrainment and center) that were considered non-significant and significant. From analyzing Table 6 it can be seen that not every cloud section measured experienced clustering that would be considered a statistical difference from a random distribution. However, a majority of the data sets do display clustering that is statistically significant, with the exception of the L1 center and H1 center data, which shows that less than 50 percent of the droplet populations display statistically significant clustering. With the exception of the L2 case (which does not have a statistical difference between edge entrainment and center clustering), that the center clustering contains a higher percentage of PCF values that are non-significant as compared to the edge entrainment data.

To develop a better understanding of the overall droplet spatial distributions and the largest inhomogeneities measured, we can directly analyze the inter-arrival time distribution (as is done in Baker (1992)). Figure 6 shows the inter-arrival distance (IAD, distance between each droplet measurement) binned for L1 and zoomed in on a frequency of 60 as to put more emphasis on the largest IAD's measured. Zooming in further on the first bin (range of 0 to 60 cm), where 98.4 percent and 99.5 percent

of the data lies for edge and center data, respectively, it can be seen that the IAD's follow a Poisson distribution. Analyzing the largest IAD's, the boxplot in the top left corner shows the data for center and edge that is  $\geq$  to the 0.998 quantile of the IAD data. This results in approximately the largest 100 IAD's to be represented in the boxplot.

Although the raw histograms of IAD data are not displayed for L2, H1, and H2 (they appear very similar in nature to that of L1), the resulting boxplots of the IAD data which is  $\geq$  to the 0.998 quantile are presented in Figure 7, where the tickmarks occurring on the upper whiskers represent the raw data positions for a better visualization of how the data is distributed. For each of the four flights, the edge data is shifted to larger IAD values as compared to the center data, with the IAD's between the edge and center data being statistically significant for each of the four cases. Note that the median value for each dataset is displayed within the boxplot. This tells us that there are more numerous, larger pockets of droplet free air within the edge zone as compared to the center zone. For example, in analyzing the boxplots for L2, we can see that there are five cases where there is a distance of 20 meters or greater between droplet measurements for the edge zone, as compared to only one case for the cloud center zone.

Figure 6 8 shows how the PCF and other environmental properties (cloud droplet number concentration ( $\text{cm}^{-3}$ ), liquid water content ( $\text{g m}^{-3}$ ), RH (%), and vertical velocity ( $\text{m s}^{-1}$ )) vary with normalized cloud height from the Case Flight. Variable quantities for each normalized cloud height can be found in Table 7. The liquid water content (LWC) increases from cloud base ( $0.073 \text{ g m}^{-3}$ ) to a normalized cloud height of 0.7 ( $0.98 \text{ g m}^{-3}$ ) before decreasing to  $0.23 \text{ g m}^{-3}$  at cloud top. Accompanied by the decrease in LWC is a sharp decrease in the RH from 99.74 % to 64.17 % between normalized cloud heights of 0.7 and 0.9, before increasing again at cloud top to 95.7 %. As both the LWC and RH decrease, the PCF has a sharp increase from 0.360.26 to 1.491.81 between normalized cloud heights of 0.8 and 1.0, indicating enhanced clustering at cloud top. The PCF values at cloud top (between normalized cloud heights of 0.8 to 1.0) are statistically significant as compared to the PCF values below a normalized altitude of 0.8 (with a p-value of 0.043), making clustering that is present at cloud top statistically significant from the clustering that is occurring in lower cloud layers.

Panel (a) gives the cloud drop size distribution for each normalized cloud height while Panel (b) gives the median droplet diameter along with the 5<sup>th</sup> and 95<sup>th</sup> percent quantiles of the drop size distribution. The median drop size increases from  $8.2911.88 \mu\text{m}$  at cloud base to  $19.6717.65 \mu\text{m}$  at cloud top. In comparing the median drop size to the mean PCF value for each normalized height, the R-squared value is 0.0410.07, indicating no correlation between the PCF and median droplet size. Particularity at cloud top where the PCF increases, there is no associated changes in the median drop size or the quantile values of the size distribution. Panel (cd) shows that the vertical velocity is negative in the upper portion of the cloud, while an updraft is present in the lower 50 % of the cloud. Table 8 gives the p-value between every normalized cloud height for the PCF. It is important to note that PCF values between normalized cloud heights of 0.8 to 0.9 are statistically significant, making clustering that is present from a normalized cloud height of 0.9 to cloud top statistically significant from the clustering that is occurring in lower cloud layers

## 4.2 Low vs. High Pollution Clustering

Figure 79, Panels (1a) and (1b) gives the same information as in Figure 5, except for the PCF values for total low pollution (average of L1 and L2) and total high pollution (average of H1 and H2), respectively. The characteristics of the two clustering signatures are similar to that of Figure 5. The average PCF values for low and high pollution **edge entrainment** and center data can be found in Table 4, along with the 15<sup>th</sup> and 85<sup>th</sup> percent quantile values. Table 4 reveals that the mean PCF values (for both **edge entrainment** and center data) for the low pollution case are larger than the corresponding mean PCF values for the high pollution case. As can be seen in Table 5, 100 percent of the first 60 21 spatial lags are statistically significant for both average low and high pollution cases between the **edge entrainment** and center data.

The larger average clustering amount for the low pollution clouds can be seen well in Panel (2a), which shows low pollution data in green and high pollution data in gold. The boundaries of each green and gold envelopes are created by the average center (bottom of each envelope) and **edge entrainment** (top of each envelope) clustering. Low pollution clouds are clearly offset to a higher clustering amount for both average center and **edge entrainment** clustering. Panel (2b) shows the overall average of all the PCF values for low and high pollution clouds. The overall average PCF value for low pollution clouds (average of **edge entrainment** and center clustering for both L1 and L2) is 0.54, while the overall average PCF value for high pollution clouds is 0.43. Although it appears that low pollution clouds experience more clustering as compared to high pollution clouds, the difference is statistically similar. The average p-value is 0.19 0.10 for the first 60 21 spatial lags with zero percent of the data being statistically significant.

Although it appears that low pollution clouds have a non-statistically significant higher amount of clustering than high pollution clouds, further analysis shows that the higher amount of clustering in the low pollution case is due entirely to the L2 flight. Figure 108 gives the same information as Panels (2a) and (2b) in Figure 97, except for the individual flights (L1, L2, H1, H2) are shown. From analyzing Panel (a), one can see the average center and **edge entrainment** clustering for L2 (light green envelope) is beyond the range of the other three flights. The total average PCF for the clouds in L1, L2, H1, and H2 is shown in Panel (b). L2 has an average PCF value of 0.76 0.77, which is roughly twice the average PCF value (and statistically significant, see Table 89) of the other three flights, where L1 (dark green), H1 (dark gold), and H2 (light gold) have average PCF values of 0.39 0.42, 0.40 0.44, 0.46 0.43, respectively. The question of whether clustering depends on aerosol number concentration cannot confidently be answered. Although Figure 97 shows that low pollution clouds have a larger amount of clustering, statistically speaking the clustering between low and high pollution clouds is the same. Further analysis shows that L1, H1, and H2 all have statistically similar clustering values (see Table 89) with average clustering amounts that are almost identical. Flight L2 has statistically significant clustering as compared to the other three cases, and is solely responsible for causing the low pollution clouds to have a higher average PCF value than that of the high pollution clouds.

## 5 Discussion

### 5.1 Cloud Lifetime Theory and Clustering in L2

An explanation for the statistically different clustering in L2 as compared to the other three cases could be cloud age. A study by Schmeissner et al. (2015) found that dissipating clouds have five main characteristics, including: a negative buoyancy ( $m$   $s^{-2}$ ) and vertical velocity, lower LWC and cloud droplet number concentrations (CDNC) as compared to actively growing clouds, and a larger RH shell around the cumulus cloud. **Decaying clouds are also associated with the enhanced entrainment of dry air, where** Cooper and Lawson (1984) found that the LWC decreases due to entrainment as cumulus clouds deteriorate. **Lu et al. (2013) and Cheng et al. (2015) also found enhanced entrainment leads to decreases in cloud droplet concentration, droplet size, and LWC.**

Figure 119 shows box plots of vertical velocity (a), LWC (b), cloud width (c), CDNC (d), buoyancy (e), and RH (f) on the y-axis and L1, L2, H1, and H2 represented in that order on the x-axis. Red median lines represent datasets that are statistically different when compared to L2. Note that except for cloud width, each variable is represented from 1-Hz data collected during in-cloud sampling. From analyzing Figure 119 (exact median values for variables can be found in Table 910), L2 has the lowest median vertical velocity, LWC, cloud width, and CDNC, with L2 being statistically significant (p-values found in Table 1011) when compared to the other three flights **for each of the variables**. The fact that L2 has the lowest median vertical velocity reflects the fact that **the clouds in L2 are either dominated by downdrafts, or have weak updrafts, making growth unlikely have smaller positive vertical velocities than those measured in the other three flights, suggesting weaker growth potential. The A** low LWC in L2 signifies that entrainment of dry air has been occurring, resulting in the evaporation of liquid water droplets, reducing the LWC and the CDNC (Pruppacher and Klett, 1997). Although Schmeissner et al. (2015) does not discuss cloud width, clouds that are dissipating would be expected to have a smaller horizontal extent due to entrainment of dry air leading to evaporation of cloud edge droplets as compared to mature clouds.

Panel (f) gives a box plot of in-cloud RH, with L2 having the lowest (by 0.1 percent) in-cloud RH, while being statistically similar to that of L1. The red dots represent the median out-of-cloud RH (100 m before and after cloud edge). L2 is the only flight where the RH increases out of the cloud. **According to Schmeissner et al. (2015), the width of the humid shell around clouds is larger for dissolving clouds as compared to actively growing clouds.** The fact that the RH is larger, on average, outside of the clouds in L2 as compared to inside of the clouds could be a sign of a large humid shell that is surrounding the individual clouds. The humid shell results from entrainment of dry air into the cloud while moist air is detrained out of the cloud into the cloud free environment, resulting in a lower (larger) RH inside (outside) the cloud. More evidence for the large humid shell can be gathered from the vertical profiles of environmental RH reported in Table 2, where the average RH (measured out-of-cloud) for the vertical range of cloud measurements was 105.2 % for L2, while for the other flights the RH was considerably lower.

Panel (e) shows the in-cloud buoyancy, which was calculated by taking the in-cloud and out-of-cloud (100 m before and after cloud edge) virtual potential temperatures. L2 has the largest median buoyancy and is statistically significant as compared to the other three flights. The clouds in the L2 flight have five out of the six characteristics for decaying clouds, including (1) lowest vertical velocity; (2) lowest LWC; (3) lowest CDNC; (4) lowest cloud width; (5) largest humid shell. The evidence

points to the clouds in L2 to be decaying on average, and therefore to be more turbulent as dry air is mixed into the clouds causing dissipation. The statistically similar values between center and edge clustering for L2 adds to the cloud lifetime theory, as it is not only the cloud edge zone that is experiencing mixing, but the entire horizontal extent of the clouds (both edge and center zones) that are experiencing mixing and dissipation. However, one would expect the buoyancy of dissipating clouds to be negatively buoyant, not positively buoyant as is shown. Although cloud age is a good theory in describing the higher clustering amounts measured in the L2 flight, the data presented does not offer a conclusive resolution.

Aerosols can act as cloud condensation nuclei (CCN), increasing the number of droplets in clouds and decreasing the mean droplet size (Twomey, 1977). Although not shown in Figure 11, for the clouds measured in this study the median droplet size was 15.01 (L1), 11.45 (L2), 11.19 (H1) and 10.92  $\mu\text{m}$  (H2). Although L2 has roughly half the aerosol number concentration as that of H1 and H2, the droplet size for L2 is more comparable to that of the high pollution flights as compared to L1. This suggests that some physical process is resulting in the droplet sizes of L2 to be smaller than what is expected based on the reported  $N_a$  values. The most likely explanation is the entrainment of dry air leading to enhanced evaporation.

Adding to the discussion, the larger the age of a cloud the higher the typical Stokes number will be due to larger droplets (from a longer droplet growth duration), implying larger clustering values. For the clouds measured in this study, the median droplet size was 15.01 (L1), 11.45 (L2), 11.19 (H1), and 10.92  $\mu\text{m}$  (H2). Although the droplet size of each droplet population is statistically significant from one another (all p-values are  $\leq 2.32 \cdot 10^{-2}$ ), the resulting Stokes numbers for each flight (assuming a constant TKE dissipation rate of  $100 \text{ cm}^2 \text{ s}^{-3}$  are 0.018, 0.010, 0.0097, and 0.0093 for L1, L2, H1, and H2, respectively. These Stokes values are all very similar to one another, suggesting that the significant difference in clustering seen in L2 is due to increased turbulence from mixing, and not a difference in droplet size.

Other possible explanations for the increased clustering in L2 could be due to flight path or the atmospheric environment for a given flight. The flight path through the cumuli for L2 could have favored cloud edge or cloud top instead of true cloud center. Favoring cloud edge would result in measuring areas of cloud that favor a higher amount of clustering (as displayed in Figure 5), and could result in the overall larger amount of average clustering experienced. Measuring just cloud edge would result in: a lower vertical velocity, LWC and CDNC (due to evaporation from entrainment), and a shorter cloud width from not traversing the maximum diameter of the cloud. However, just as with the cloud lifetime theory, the buoyancy is expected to be negative, not positive, in the edge zone of the cloud due to evaporational cooling of the air.

Comparing cloud width on different days can become complicated due to the environmental factors that control cloud size. As is discussed in Hill (1973), the dominant factor governing the size of cumulus clouds is the size and strength of the sub-cloud circulations. There is no way to know what the sub-cloud circulation was for the given days. Only vertical velocity is available, which, as we saw from Panel (a) in Figure 119, was smallest for the in-cloud portions of the L2 flight. Whether the fact that L2 clouds were smaller as compared to the other flights is due to dissipation through entrainment of dry air or environmental characteristics is unknown.

## 5.2 Edge vs. Center Clustering and Aerosol Number Concentration

The finding that clustering is enhanced at smaller spatial/temporal scales agrees with the findings in multiple other papers, including Good et al. (2012); Ireland and Collins (2012); Saw et al. (2012). Note that in this paper clustering is measured down to  $\sim 1.82$  cm. It is expected from the inertial clustering hypothesis that clustering continues to increase at scales below what was measured here, into the millimeter scales (Shaw, 2003) due to inertial clustering from fluid vorticity. It is important to note however, that not all the clustering measured was statistically different from a random poisson distribution. Only 60.8 % of the traverses for center data showed a statistical deviation from a randomly distributed droplet population, as compared to 72.2% for edge data. This suggests that although a majority of the data displays large-scale inhomogeneity, 31.7 % of the data are randomly distributed. This is partially in agreement with Chaumat and Brenguier (2001), which found that droplets displayed homogeneous distributions on small and large scales.

PCF curves measuring inertial clustering in other literature (Larsen, 2007; Shaw, 2003; Shaw et al., 2002) show an elevated value of the PCF at the smallest separations that is naturally accompanied with lower values of the PCF at larger separations. The PCF curves presented here are measured over separations ranging from 1.82 cm (just above the Kolmogorov scale) to 12 m (on the order of the integral scale) and show elevated values over a large spatial range (1.82 cm to 60 cm) before the PCF begins to decay. It is important to keep in mind that this suggests that the elevated PCF values examined here between 12 to 60 cm are the result of spatial holes in the droplet concentrations (non-stationary) due to mixing with dryer air, and not preferential concentration from particle inertia. Note that other possible causes of larger scale inhomogeneity that are not examined here include fluctuations in the vertical velocity and cloud condensation nuclei (Pinsky and Khain, 2002, 2003).

From the clouds measured, the conclusion can be made that droplet clustering does change as a function of cloud center vs. cloud edge entrainment, with a larger amount of clustering being non-Poissonian, as seen in Table 6 with the edge entrainment zone having a larger amount of clustering than the center of the cloud, which is shown to be statistically significant. The decrease in clustering in the center of the cloud as compared to the edge may be attributed to several aspects, including (1) the mean entrainment rate decreases from cloud edge to cloud center, as has been shown with in-situ measurements made by Cheng et al. (2015). (2) Turbulent mixing within the cloud leads to a breakup of the larger-scale clustering, reducing the PCF. Ireland and Collins (2012) through simulations observed a larger degree of non-uniformity for a turbulent-non-turbulent interface (i.e., cloud edge) as compared to a turbulent-turbulent interface (i.e., cloud center) due to the lower turbulence levels at the edge weakening the homogenization process of the clustering. Entrainment is the process by which sub-saturated air surrounding a cloud is drawn into the cloud due to the turbulent motions of the cloudy air, leading to a decrease in the LWC and RH. Cloud top entrainment is evident from looking at Figure 8, Panel (b), which shows the RH and LWC decreasing near cloud top. The entrainment at cloud top can be seen to cause a negative vertical velocity (from evaporative cooling) in the upper portion of the cloud (Figure 8, Panel (c)), where the average vertical velocity is increasingly negative above a normalized cloud height of 0.5, suggesting penetrative downdrafts extend into the middle section of the cloud. Accompanying the cloud top entrainment is a clear increase in the clustering amount.

The production of turbulent energy is equal to the rate of viscous dissipation. Since both production and dissipation depend on the rate of strain  $s_{ij}$  (Tennekes and Lumley, 1972), and droplet clustering also depend on  $s_{ij}$  from Equation 1, this suggests that droplet clustering depends on turbulence. It was also discussed in Section 2.1 that the Stokes number, which effects the clustering amount, depends on the turbulent dissipation rate. Smith and Jonas (1995) found that the dominant TKE source was at cloud top and was interpreted as evidence for the cloud–top entrainment instability process which produced observed strong downdrafts at cloud top. Shaw (2003) states that one of the main sources of TKE in clouds is from shear evaporative cooling at cloud edge and cloud top. Kitchen and Caughey (1981) found that turbulent dissipation rates were twice as large at cloud top, which can also be inferred for cloud edge as well.

The findings from previous papers that turbulence is enhanced at cloud top and edge, on top of the fact that entrainment is defined as a mixing process, which in turn is turbulent, could be a possible explanation for the enhanced clustering that is observed in entrainment and cloud top zones. Unfortunately, the turbulent dissipation rate was not measured in this study due to the lack of 3–D wind data. This work therefore has the potential to be expanded upon by measuring the turbulent dissipation rate and droplet clustering, and determining if there is a strong correlation. Keep in mind that the results presented here provide an overall statistical look at how droplet clustering changes with cloud edge, center, and top, and provides some theories as to how the clustering measured may be related to turbulence. However, the overall numerical values obtained should not be used quantitatively for precipitation modeling since the data used is non–stationary, and comes from a source (cumulus clouds) that are not known to be stationary.

Along with enhanced clustering at cloud edge, enhanced clustering at cloud top is also evident due to entrainment as is shown in Figure 8, where the LWC and RH have a sharp decrease near cloud top accompanied by an increase in the PCF. The decrease in RH and LWC is characteristic of dry air being entrained into the cloud. The entrainment at cloud top can also be seen to cause a negative vertical velocity (from evaporative cooling, typically termed cloud–top entrainment instability) in the upper portion of the cloud (Figure 8, Panel (c)), where the average vertical velocity is increasingly negative above a normalized cloud height of 0.5, suggesting penetrative downdrafts extend into the middle section of the cloud.

Although the conclusion in this paper is that aerosol number concentration does not affect droplet clustering, this conclusion can only be made for the range of  $N_a$  given and the resulting mean droplet sizes. For example, Xue and Feingold (2006) showed that smaller droplets evaporate more readily, leading to dissipation of the cloud through entrainment. However, in Xue and Feingold (2006) the difference in droplet size was roughly -81 % between clean and polluted clouds. Although the difference in droplet size is statistically significant between flights, the largest percent difference analyzed here is only -28 % between flights L1 and H2. Perhaps the aerosol number concentration can affect the amount of clustering that is occurring if there are more significant changes in the sizes of the droplet populations than those analyzed here. Such a case could be comparing a highly polluted cloud in Houston (mean droplet diameter  $\sim 11 \mu\text{m}$ ) to a clean cloud over the ocean (mean droplet diameter  $\sim 35 \mu\text{m}$ , as was found for some Atlantic trade wind cumuli (Wang et al., 2009)). This would result in droplet populations that have a large enough percent different in their size that evaporative effects may be severe enough to lead to statistically different entrainment rates and droplet clustering. However, sampling clouds in two different types of boundary layers would result in vast differences in their environmental characteristics. One way in which sampling could be achieved

would be to analyze cumuli that are exposed to a point source of pollution (such as volcanic gas emissions in Hawaii) in the marine boundary layer and cumuli that lie outside the pollution plume. This would allow for the sampling of clouds which are exposed to vast differences in  $N_a$  but still share many of the same environmental characteristics.

### 5.3 Aerosol Number Concentration

5 The results show that the clustering between low and high pollution clouds is statistically similar, suggesting that clustering does not depend on the aerosol number concentration. However, the Stokes number (Equation 3) depends on (1) turbulent dissipation; (2) droplet size. Even though the droplet sizes between low and high pollution clouds are statistically different, they are still too similar in size (13.4  $\mu\text{m}$  for low and 10.7  $\mu\text{m}$  for high) to produce significant differences in  $S_t$ . For example, assuming the two mean droplet diameters and a turbulent dissipation rate of  $100 \text{ cm}^2 \text{ s}^{-3}$ , a Stokes Number of 0.036 and 0.023  
10 for low and high pollution data, respectively, is obtained. Both Stokes numbers are  $\ll 1$ , resulting in the droplets following the fluid flow very accurately.

Perhaps the aerosol number concentration can affect the amount of clustering that is occurring if there are significant changes in the sizes of the droplet populations. Such a case could be comparing a highly polluted cloud in Houston (mean droplet diameter  $\sim 11 \mu\text{m}$ ) to a clean cloud over the ocean (mean droplet diameter  $\sim 35 \mu\text{m}$ , as was found for some Atlantic trade wind  
15 cumuli (Wang et al., 2009)). Assuming the Turbulent dissipation rate is constant at  $100 \text{ cm}^2 \text{ s}^{-3}$ , the Stokes number for the polluted cloud would be 0.024, while for the Atlantic trade wind cumuli it would be 0.243, a full order of magnitude greater. A cloud with a mean droplet diameter of  $50 \mu\text{m}$  would result in a Stokes number of 0.49. Per Equation 4, a monotonic increase of droplet clustering occurs with increasing Stokes number. Although different authors have come to different conclusions on the exact increase in droplet clustering with different Stokes numbers using direct numerical simulations, it has been found  
20 that for a range of  $S_t \ll 1$  to  $S_t = 0.25$  that the PCF can vary between near homogeneous (zero) amounts of droplet clustering at the lower limit and values between one and two at the upper limit (Chun and Koch, 2005; Wang et al., 2000; Falkovich and Pumir, 2004). This suggests that the large range of droplet sizes experienced between highly polluted and clean maritime clouds can result in Stokes number differences that produce significant differences in clustering signatures, although this has not been observed/measured in naturally occurring clouds to this point.

25 Although the conclusion in this paper is that aerosol number concentration does not affect droplet clustering, this conclusion can only be made for the range of  $N_a$  given and the resulting mean droplet sizes. From Equation 4, the aerosol number concentration can affect droplet clustering, given there is a large enough difference in mean droplet size from the aerosol forcing. Also, consider that the droplet size can influence the entrainment rate from increased evaporation of smaller droplets, impacting the turbulent dissipation rate.

## 30 6 Conclusions

Flight data obtained from the CIRPAS Twin otter aircraft flown during the GoMACCS campaign near Houston, TX from 2006 were used to investigate 81 non-precipitating cumulus clouds, and one vertically developed cumulus cloud, to better understand

how droplet clustering changes as a function of cloud location (cloud edge vs. cloud center) and aerosol number concentration. Of the 22 flights flown, two low (L1, L2) and high (H1, H2) pollution flights were selected to analyze how droplet clustering changed with aerosol number concentration.

It has been shown that (1) droplet clustering is enhanced at cloud edge (and cloud top) as compared to cloud center (statistically significant), with a statistically significant difference between cloud edge and center. Most of and the clustering measured is shown to be real, physical variability (non-Poissonian). Statistically significant enhanced clustering is also shown at cloud top as compared to the lower portion of the cloud. (2) There is no statistical difference at the 5 percent level for droplet clustering between low and high pollution clouds, at least for the range of  $N_a$  that was measured in this research. Although it was found that low pollution clouds do, on average, have a larger amount of clustering in both the center and edge zones, this is due entirely to the L2 flight. (3) L1, H1, and H2 have a statistically similar amount of clustering at the 5 percent level, while L2 has a larger, statistically significant amount of clustering. It is proposed that cloud age plays an important role in the amount of clustering that is occurring, with decaying clouds demonstrating a higher amount of clustering as compared to developing clouds due to enhanced entrainment of dry air, although this theory needs more work as the buoyancy data is not in agreement for decaying clouds.

This work provides a good statistical base for analyzing how droplet clustering changes with cloud location and aerosol number concentration, keeping in mind that using the results presented here for quantitative purposes is not wise due to the non-stationarity of the data. The conclusions from this work are drawn only from 81 clouds whose properties are highly variable and influenced by environmental aspects that are not constrained by the observations, including the sub-cloud layer properties and the lifecycle stage of the clouds. This study examined the cloud properties at instantaneous moments, resulting in a mean behaviour averaged over each cloud and each flight. Further analysis and data from more clouds is required to confirm some of the ideas that have been presented here. For example, if a field campaign takes place in the future for the purposes of illuminating these results, constraints on the lifecycle stage of the observed clouds must be considered, along with the proper instrumentation for turbulent analysis.

*Author contributions.* Both authors contributed equally to both the analysis and the writing of this manuscript.

*Competing interests.* There are no competing interests to declare

*Acknowledgements.* We thank Hafliði Jonsson and Patrick Chuang for their support during the original field campaign. We also thank the CIRPAS Twin Otter crew and personnel for their effort and support during the field program and John Seinfeld and Rick Flagan (Caltech) and their research groups for assistance and discussions in the field regarding other GoMACCS data sets. Michael Larsen (College of Charleston)

also deserves thanks for his suggestions and intellectual help which made this paper possible. This work was funded by NSF CAREERS grant 1255649.

## References

- Baker, B.: Turbulent Entrainment and Mixing in Clouds: A New Observation Approach, *J. Atmos. Sci.*, 49, 387–404, 1992.
- Baker, B. A. and Lawson, R. P.: Analysis of Tools used to Quantify Droplet Clustering in Clouds, *J. Atmos. Sci.*, <https://doi.org/10.1175/2010JAS3409.1>, 2010.
- 5 Baker, M., Corbin, R., and Latham, J.: The influence of entrainment on the evolution of cloud droplet spectra: I. A model of inhomogeneous mixing, *Quart. J. Roy. Meteor. Soc.*, 106, 581–598, 1980.
- Baker, M., Breidenthal, R., Choullarton, T., and Latham, J.: The effects of turbulent mixing in clouds, *J. Atmos. Sci.*, 41, 209–304, 1984.
- Brenguier, J.: Observations of cloud microstructure at the centimeter scale, *J. Appl. Meteor.*, 32, 783–793, 1993.
- Chaumat, L. and Brenguier, J.: Droplet Spectra Broadening in Cumulus Clouds. Part II: Microscale Droplet Concentration Heterogeneities, *J. Atmos. Sci.*, 58, 642–654, 2001.
- 10 Cheng, M., Lu, C., and Liu, Y.: Variation in entrainment rate and relationship with cloud microphysical properties on the scale of 5 m, *Sci. Bull.*, 60, 707–717, 2015.
- Chuang, P. Y., Saw, E. W., Small, J. D., Shaw, R. A., Sopperley, C. M., Payne, G. A., and Bachalo, W. D.: Airborne Phase Doppler Interferometry for Cloud Microphysical measurements, *Aerosol Sci. Tech.*, 42, 685–703, 2008.
- 15 Chun, J. and Koch, D. L.: Coagulation of monodisperse aerosol particles by isotropic turbulence, *Phys. Fluid*, 17, 27 102–1–27 102–5, 2005.
- Cooper, W. A. and Lawson, R. P.: Physical interpretation of results from HIPLEX-1 Experiment, *J. Climate Appl. Meteor.*, 23, 532–540, 1984.
- Eaton, J. K. and Fessler, J. R.: Preferential concentration of particles by turbulence, *Int. J. Multiphase Flow*, 20, 169–209, 1994.
- Falkovich, G. and Pumir, A.: Intermittent distribution of heavy particles in a turbulent flow, *Phys. Fluid*, 16, L47–L50, 2004.
- 20 Feingold, G., Frisch, A. S., Stevens, B., and Cotton, W. R.: On the relationship among cloud turbulence, droplet formation and drizzle as viewed by Doppler radar, microwave radiometer, and lidar, *J. Geophys. Res.*, 104, 22 195–22 203, 1999.
- Fouxon, I., Park, Y., Harduf, R., and Lee, C.: Inhomogeneous distribution of water droplets in cloud turbulence, *Phys. Rev. E*, 92, 033 001, 2015.
- Gerber, H. E., Frick, G. M., Jensen, J. B., and Hudson, J. G.: Entrainment, mixing, and microphysics in trade-wind cumulus, *J. Met. Soc. Japan*, 86A, 87–106, 2008.
- 25 Good, G., Gerashchenko, S., and Warhaft, Z.: Intermittency and inertial particle entrainment at a turbulent interface: the effect of the large-scale eddies, *J. Fluid Mech.*, 694, 371–398, 2012.
- Grabowski, W. and Clark, T.: Cloud–environment interface instability: Rising thermal calculations in two spatial dimensions, *J. Atmos. Sci.*, 48, 527–546, 1993.
- 30 Grabowski, W. and Vaillancourt, P.: Comments on "Preferential concentration of cloud droplets by turbulence: Effects on the early evolution of cumulus cloud droplet spectra", *J. Atmos. Sci.*, 56, 1433–1436, 1999.
- Grabowski, W. and Wang, L.: Growth of Cloud Droplets in a Turbulent Environment, *Annu. Rev. Fluid Mech.*, 45, 293–324, 2013.
- Grabowski, W. W. and Wang, L. P.: Diffusion and accretional growth of water drops in a rising adiabatic parcel: effects of the turbulent collision kernel, *Atmos. Chem. Phys.*, 9, 2335–2353, 2009.
- 35 Hill, G. E.: Factors controlling the size and spacing of cumulus clouds as revealed by numerical experiments, *J. Atmos. Sci.*, 31, 646–673, 1973.

- Hogan, R. C. and Cuzzi, J. N.: Stokes and reynolds number dependence of preferential concentration in simulated three-dimensional turbulence, *Phys. Fluids*, 13, 2938–2945, 2001.
- Holtzer, G. L. and Collins, L. R.: Relationship between the intrinsic radial distribution function for an isotropic field of particles and lower-dimensional measurements, *J. Fluid Mech.*, 459, 93–102, 1997.
- 5 Hunt, J., Eames, I., and Westerweel, J.: Mechanics of inhomogeneous turbulence and interfacial layers, *J. Fluid Mech.*, 554, 499–519, 2006.
- Ireland, P. and Collins, L.: Direct numerical simulation of inertial particle entrainment in a shearless mixing layer, *J. Fluid Mech.*, 704, 301–332, 2012.
- Jonas, P.: Turbulence and cloud microphysics, *Atmos. Res.*, 40, 283–306, 1996.
- Jonas, P. R. and Mason, B. J.: Entrainment and the droplet spectrum in cumulus clouds, *Quart. J. Roy. Meteor. Soc.*, 108, 857–869, 1982.
- 10 J. Warner: The microstructure of cumulus cloud: Part II: The effect on droplet size distribution of the cloud nucleus spectrum and updraft velocity, *J. Atmos. Sci.*, 26, 1035–1040, 1969.
- Kang, H. and Meneveau, C.: Experimental study of an active grid-generated shearless mixing layer and comparisons with large-eddy simulation, *Phys. Fluids*, 20, 125–102, 2008.
- Khain, A., Ovtchinnikov, M., Pinsky, M., Pokrovsky, A., and Krugliak, H.: Notes on the state-of-the-art numerical modeling of cloud  
15 microphysics, *Atmos. Res.*, 55, 159–224, 2000.
- Kitchen, M. and Caughey, S. J.: Tethered-balloon observed observations of the structure of small cumulus clouds, *Q.J.R. Meteorol. Soc.*, 107, 853–874, 1981.
- Knight, C. A., Vivekanandan, J., and Lasher-Trapp, S. G.: First Radar Echoes and the Early Zdr History of Florida Cumulus, *J. Atmos. Sci.*, 297, 1667–1670, 2002.
- 20 Kogan, Y. L.: Drop Size Separation in Numerically Simulated Convective Clouds and Its Effect on Warm Rain Formation, *J. Atmos. Sci.*, 50, 1238–1253, 1993.
- Kostinski, A. B. and Jameson, A. R.: Fluctuation properties of precipitation. Part 1. On Deviations of Single-Size Drop Counts from the Poisson Distribution, *J. Atmos. Sci.*, 54, 2174–2186, 1997.
- Kostinski, A. B. and Shaw, R. A.: Scale dependent droplet clustering in turbulent clouds, *J. Fluid Mech.*, 434, 389–398, 2001.
- 25 Krueger, S. K., Su, C.-W., and McMurtry, P. A.: Modeling entrainment and finescale mixing in cumulus clouds, *J. Atmos. Sci.*, 54, 2697–2712, 1997.
- Laird, N. F., Ochs, H. T., Rauber, R. M., and Miller, L. J.: Initial Precipitation Formation in Warm Florida Cumulus, *J. Atmos. Sci.*, 57, 3740–3751, 2000.
- Langmuir, I.: *J. Atmos. Sci.*, 5, 175–192, 1948.
- 30 Larsen, M.: Spatial distributions of aerosol particles: Investigation of the Poisson assumption, *Aerosol Sci.*, 38, 807–822, 2007.
- Larsen, M.: Scale Localization of Cloud Particle Clustering Statistics, *J. Atmos. Sci.*, 69, 3277–3289, 2012.
- Larsen, M. L. and Kostinski, A. B.: Observations and Analysis of Uncorrelated Rain, *J. Atmos. Sci.*, 62, 4071–4083, 2005.
- Lehmann, K., Siebert, H., Wendisch, M., and Shaw, R.: Evidence for Inertial droplet clustering in weakly turbulent clouds, *Tellus B*, 59, 57–65, 2007.
- 35 Lehmann, K., Siebert, H., and Shaw, R. A.: Homogeneous and Inhomogeneous Mixing in Cumulus Clouds: Dependence on Local Turbulence Structure, *J. Atmos. Sci.*, 66, 3641–3659, 2009.
- Lu, C., Niu, S., Liu, Y., and Vogelmann, A.: Empirical relationship between entrainment rate and microphysics in cumulus clouds, *Geophys. Res. Lett.*, 60, 2333–2338, 2013.

- Lu, M., Jonsson, H., Chuang, P., Feingold, G., and Flagan, R.: Aerosol–cloud relationships in continental shallow cumulus, *J. Geophys. Res.*, 113, D15 201, 2008.
- MacPherson, J. I. and Isaac, G. A.: Turbulent characteristics of some Canadian cumulus clouds, *J. Appl. Met.*, 16, 81–90, 1977.
- Marshak, A., Knyazikhin, Y., Larsen, M. L., and Wiscombe, W.: Small–Scale Drop Variability: Empirical Models for Drop–Size–Dependent Clustering in Clouds, *J. Atmos. Sci.*, 62, 551–558, 2005.
- Maxey, M. R.: The gravitational settling of aerosol particles in homogeneous turbulence and random flow fields, *J. Fluid Mech.*, 174, 441–465, 1987.
- Moghadaripour, M., Azimi, A. H., and Glyasi, S.: Experimental study of oblique particle clouds in water, *Int. J. of Multiphase Flow*, 91, 101–119, 2017.
- 10 Paluch, I. and Baumgardner, D.: Entrainment and fine–scale mixing in a continental convective cloud, *J. Atmos. Sci.*, 46, 261–278, 1989.
- Picinbono, B. and Bendjaballah, C.: Characterization of nonclassical optical fields by photodetection statistics, *Phys. Rev. A*, 71, 1–12, 2005.
- Pinsky, M. and Khain, A.: Fine Structure of cloud droplet concentration as seen from the Fast–FSSP Measurements. Part II: Results of In Situ Observations, *J. Appl. Meteor.*, 42, 65–73, 2003.
- Pinsky, M., Khain, A., and Shapiro, M.: Collision of Small Drops in a Turbulent Flow. Part I: Collision Efficiency. Problem Formulation and Preliminary Results, *J. Atmos. Sci.*, 56, 2585–2600, 1999.
- 15 Pinsky, M., Khain, A., and Krugliak, H.: Collisions of cloud droplets in a turbulent. Part V: Application of detailed tables of turbulent collision rate enhancement to simulation of droplet spectra evolution, *J. Atmos. Sci.*, 65, 357–374, 2008.
- Pinsky, M. B. and Khain, A. P.: Effect of in–cloud nucleation and turbulence on droplet spectrum formation in cumulus clouds, *Q. J. R. Meteorol. Soc.*, 128, 501–533, 2002.
- 20 Pinsky, M. B., Khain, A., and Shapiro, M.: Collisions of Cloud Drops in a Turbulent Flow. Part IV: Droplet Hydrodynamic Interaction, *J. Atmos. Sci.*, 64, 2462–2482, 2006.
- Pruppacher, H. and Klett, J.: *Microphysics of clouds and precipitation*, Kluwer Academic Publishers, 2 edn., 1997.
- Ramaswamy, V., Boucher, O., Haigh, J., Hauglustaine, D., Haywood, J., Myhre, G., Nakajima, T., Shi, G. Y., and Solomon, S.: Radiative forcing of climate change, in: *Climate Change: 2001: The Scientific Basis. Contribution of working group I to the Third Assessment Report of the Intergovernmental Panel on Climate Change*, Cambridge Univ. Press, 2001.
- 25 Rogers, R. R. and Yau, M. K.: *A Short Course in Cloud Microphysics*, Pergamon Press, 3 edn., 1989.
- Rosenfeld, D., Lahav, R., Khain, A., and Pinsky, M.: The Role of Sea Spray in Cleansing Air Pollution over Ocean via Cloud Processes, *Science*, 297, 1667–1670, 2002.
- Rosenfeld, D., Lohmann, U., Raga, G. B., O’Dowd, C. D., Fuzzi, S., Reissell, A., and Andreae, M. O.: Flood or Drought: How Do Aerosols Affect Precipitation, *Science*, 321, 1309–1313, 2008.
- 30 Saffman, P. G. and Turner, J. S.: On the collision of drops in turbulent clouds, *J. Fluid Mech.*, 30, 1–16, 1956.
- Saw, E.: *Studies of spatial clustering of inertial particles in turbulence*, Ph.D. thesis, Michigan Technological University, 2008.
- Saw, E., Shaw, R., Salazar, J., and Collins, L.: Spatial clustering of polydisperse inertial particles in turbulence: II. Comparing simulation with experiment, *New Journal of Physics*, 14, 105 031, 2012.
- 35 Saw, E. W., Shaw, R. A., Ayyalasomayajula, S., Chuang, P. Y., and Gyfason, A.: Inertial Clustering of Particles in High Reynolds–Number Turbulence, *Phys. Rev. Lett.*, 100, 214 501, 2008.
- Schmeissner, T., Shaw, R. A., Ditas, J., Strathmann, F., Wendisch, M., and Siebert, H.: Turbulent mixing in shallow Trade Wind cumuli: dependence on cloud life cycle, *J. Atmos. Sci.*, 72, 1447–1465, 2015.

- Seifert, A., Nuijens, L., and Stevens, B.: Turbulence effects on warm-rain autoconversion in precipitating shallow convections, *Quart. J. Roy. Meteor. Soc.*, 136, 1753–1762, 2010.
- Shaw, R. A.: Particle–Turbulence Interactions in Atmospheric Clouds, *Annu. Rev. Fluid Mech.*, 35, 183–227, 2003.
- Shaw, R. A., Reade, W. C., Collins, L. R., and Verlinde, J.: Preferential Concentration of Cloud Droplets by Turbulence: Effects on the Early Evolution of Cumulus Cloud Droplet Spectra, *J. Atmos. Sci.*, 55, 1965–1976, 1998.
- Shaw, R. A., Kostinski, A. B., and Larsen, M. L.: Towards quantifying droplet clustering in clouds, *Q. J. Roy. Meteor. Soc.*, 128, 1043–1057, 2002.
- Siebert, H., Lehmann, K., and Wendisch, M.: Observations of small-scale turbulence and energy dissipation rates in the cloudy boundary layer, *J. Atmos. Sci.*, 63, 1451–1466, 2006.
- 10 Siebert, H., Gerashchenko, S., Gylfason, A., Lehmann, K., Collins, L. R., Shaw, R. A., and Warhaft, Z.: Toward understanding the role of turbulence on droplets in clouds: In situ and laboratory measurements, *Atmos. Res.*, 97, 426–437, 2010.
- Small, J. D., Chuang, P., Feingold, G., and Jiang, H.: Can aerosol decrease cloud lifetime?, *Geophys. Res. Lett.*, 36, L16 806, 2009.
- Small, J. D., Chuang, P. Y., and Jonsson, H. H.: Microphysical imprint of entrainment in warm cumulus, *Tellus B*, 65, 1–18, 2013.
- Smith, S. A. and Jonas, P. R.: Observations of the turbulent fluxes in fields of cumulus clouds, *Z.J.R. Meteor. Soc.*, 85, 144–151, 1995.
- 15 Squires, K. and Eaton, J.: Measurements of particle dispersion from direct numerical simulations of isotropic turbulence, *J. Fluid Mech.*, 226, 1–35, 1991.
- Srivastava, R. C.: Growth of Cloud Drops by Condensation: A Criticism of Currently Accepted Theory and a New Approach, *J. Atmos. Sci.*, 46, 869–887, 1989.
- Stein, A. F., Draxler, R. R., Rolph, G. D., Stunder, B. J., Cohen, M. D., and Ngan, F.: HYSPLIT atmospheric transport and dispersion modeling system, *Bull. Amer. Meteor. Soc.*, 96, 2059–2077, 2015.
- 20 Sundaram, S. and Collins, L. R.: Collision statistics in an isotropic particle–laden turbulent suspension. Part I. Direct numerical simulations, *J. Fluid. Mech.*, 335, 75–109, 1997.
- Szumowski, M. J., Rauber, R. M., III, H. T. O., and Miller, L. J.: The Microphysical Structure and Evolution of Hawaiian Rainband Clouds. Part I: Radar Observations of Rainbands Containing High Reflectivity Cores, *J. Atmos. Sci.*, 48, 112–121, 1997.
- 25 Telford, J. W. and Chai, S. K.: A new aspect of condensation theory, *Pure Appl. Geophys*, 118, 720–742, 1980.
- Tennekes, J. and Lumley, J. L.: *A First Course in Turbulence*, The MIT press, 1972.
- Twomey, S.: The Influence of pollution on the shortwave albedo of clouds, *J. Atm. Sci.*, 34, 1149–1152, 1977.
- Vaillancourt, P. A., Yau, M. K., and Bartello, P.: Microscopic Approach to Cloud Droplet Growth by Condensation. Part II: Turbulence, Clustering, and Condensational Growth, *J. Atmos. Sci.*, 59, 3421–3435, 2002.
- 30 vanZanten, M. C., Stevens, B., Nuijens, L., Siebesma, A., Ackerman, A., Burnet, F., Cheng, A., Couvreux, F., Jiang, H., Khairoutdinov, M., Kogan, Y., Lewellen, D., Mechem, D., Nakamura, K., Noda, A., Shipway, B., Slawinska, J., Wang, S., and Wyszogrodzki, A.: Controls on precipitation and cloudiness in simulations of trade–wind cumulus as observed during RICO, *J. Adv. Model. Earth Syst.*, 3, M06 001, 2011.
- Veeravalli, S. and Warhaft, V.: The shearless turbulence mixing layer, *J. Fluid Mech.*, 207, 191–229, 1989.
- 35 Wang, L.-P. and Maxey, M. R.: Settling velocity and concentration distribution of heavy particles in homogeneous isotropic turbulence, *J. Fluid. Mech.*, 256, 27–68, 1993.
- Wang, L.-P., Wexler, A. S., and Zhou, Y.: Statistical mechanical description and modeling of turbulent collision of inertial particles, *J. Fluid Mech.*, 415, 117–153, 2000.

- Wang, Y., Geerts, B., and French, J.: Dynamics of the cumulus cloud margin: An observational Study, *J. Atmos. Sci.*, 66, 3660–3677, 2009.
- Wilks, D. S.: Statistical methods in the atmospheric sciences, vol. 100 of *International Geophysics Series*, Academic Press, 3 edn., 2011.
- Wood, A. M., Hwang, W., and Eaton, J. K.: Preferential concentration of particles in homogeneous and isotropic turbulence, *Int. J. of Multiphase Flow*, 31, 1220–1230, 2005.
- 5 Wyszogrodzki, A. A., Grabowski, W. W., Wang, L. P., and Ayala, O.: Turbulent collision–coalescence in maritime shallow convection, *Atmos. Chem. Phys.*, 13, 8471–8487, 2013.
- Xue, H. and Feingold, G.: Large–Eddy Simulations of Trade Wind Cumuli: Investigation of Aerosol Indirect Effects, *J. Atmos. Sci.*, 63, 1605–1622, 2006.
- Zhou, Y., Wexler, A. S., and Wang, L.-P.: Modelling turbulent collision of bidisperse inertial particles, *J. Fluid Mech.*, 433, 77–104, 2001.

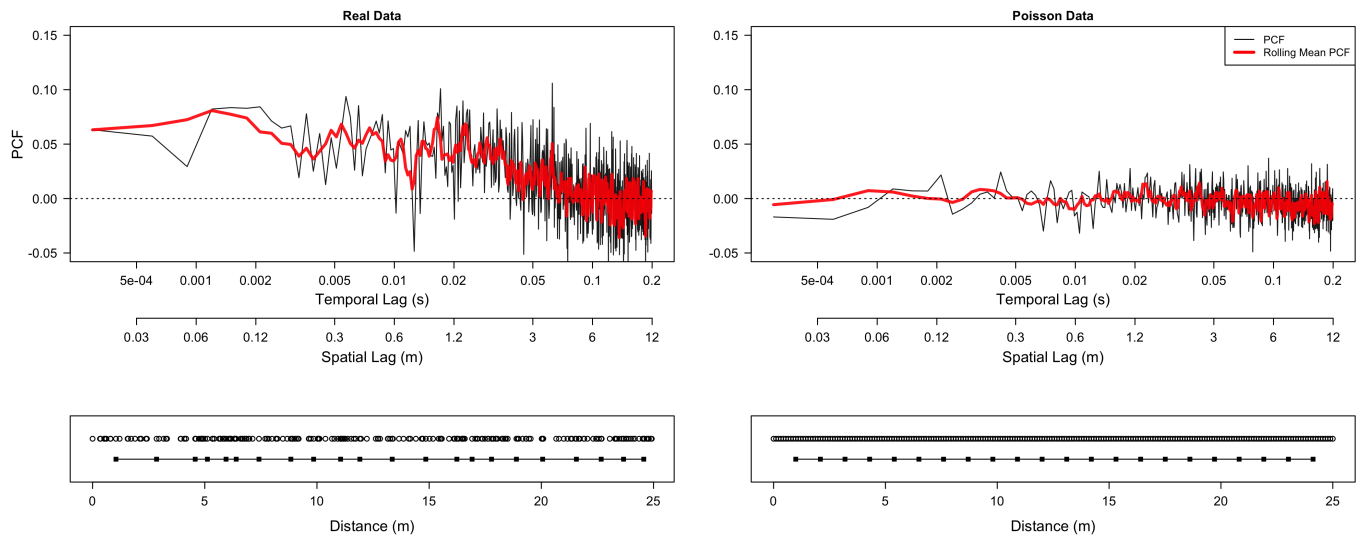


**Figure 1.** Top panels represent the clustering signature for the PCF, with the x-axis showing the temporal and spatial lag on a log-scale and the y-axis representing the PCF (unitless). The top-left shows the PCF for data from a randomly selected portion of cloud covering a temporal range of 2 seconds ( $\sim 120$  m) with a population of 2168 droplets. The top-right panel shows simulated Poisson point data with the same temporal scale and droplet population. The red line represents a rolling mean of five for the raw PCF values (shown in black). The bottom panels represent short 25 m subsets ( $\sim 270$  droplets) of the data used in generating the PCF curves. Each circle represents a cloud droplet, and each line with a square represents the distance traversed for each sampling volume, with each square corresponding to a droplet count of 10.

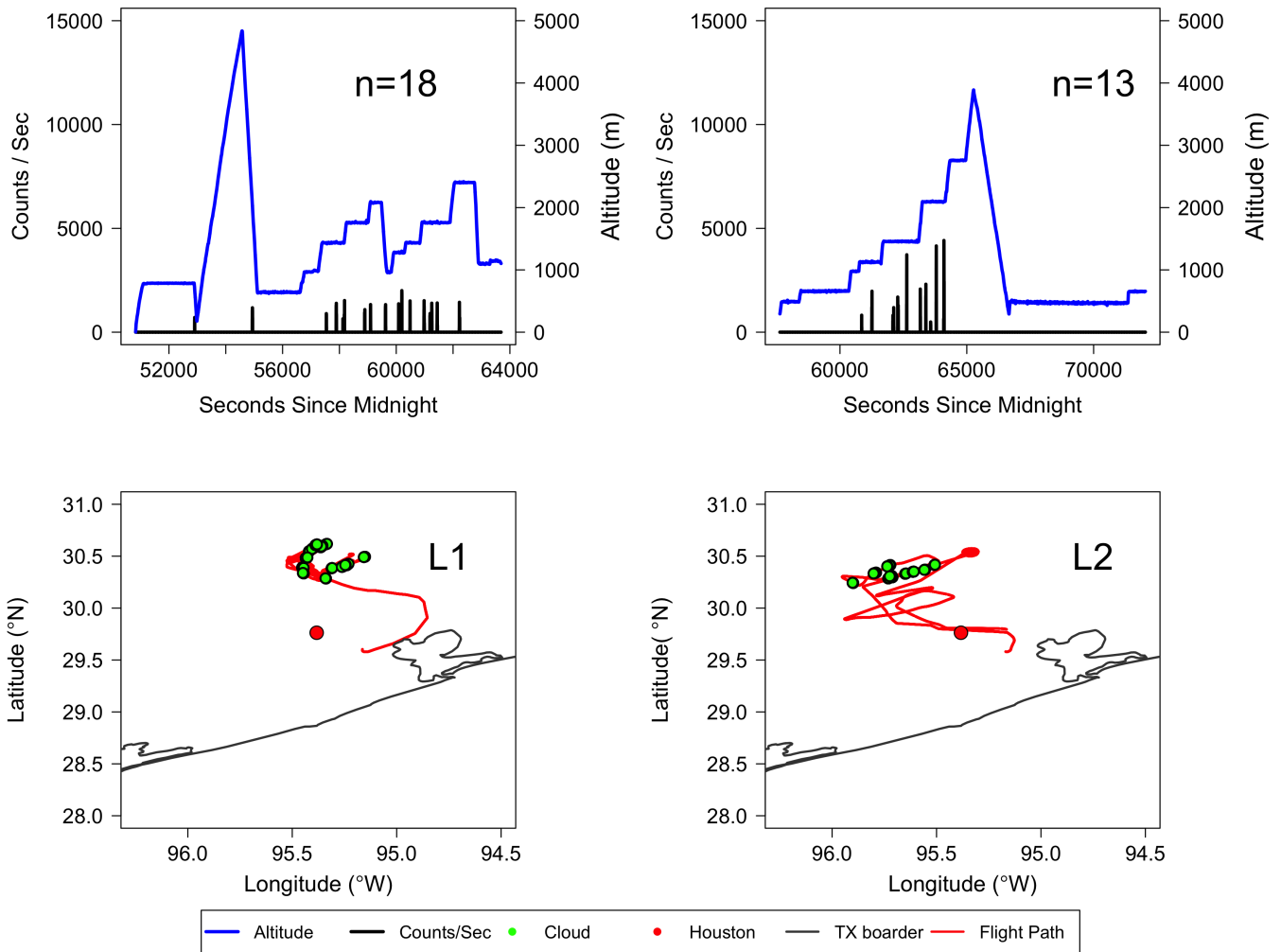


**Figure 2.** Shows L1 and L2 on the left and right, respectively. Flight altitude (blue) as a function of time is displayed in the top panels, with droplet counts per second in black. The “n=” represents the number of clouds sampled for each flight after filtering. The bottom panels show the Texas coast in grey with the location of Houston represented by the red dot. The flight path is outlined in red with the location of clouds displayed by green dots.

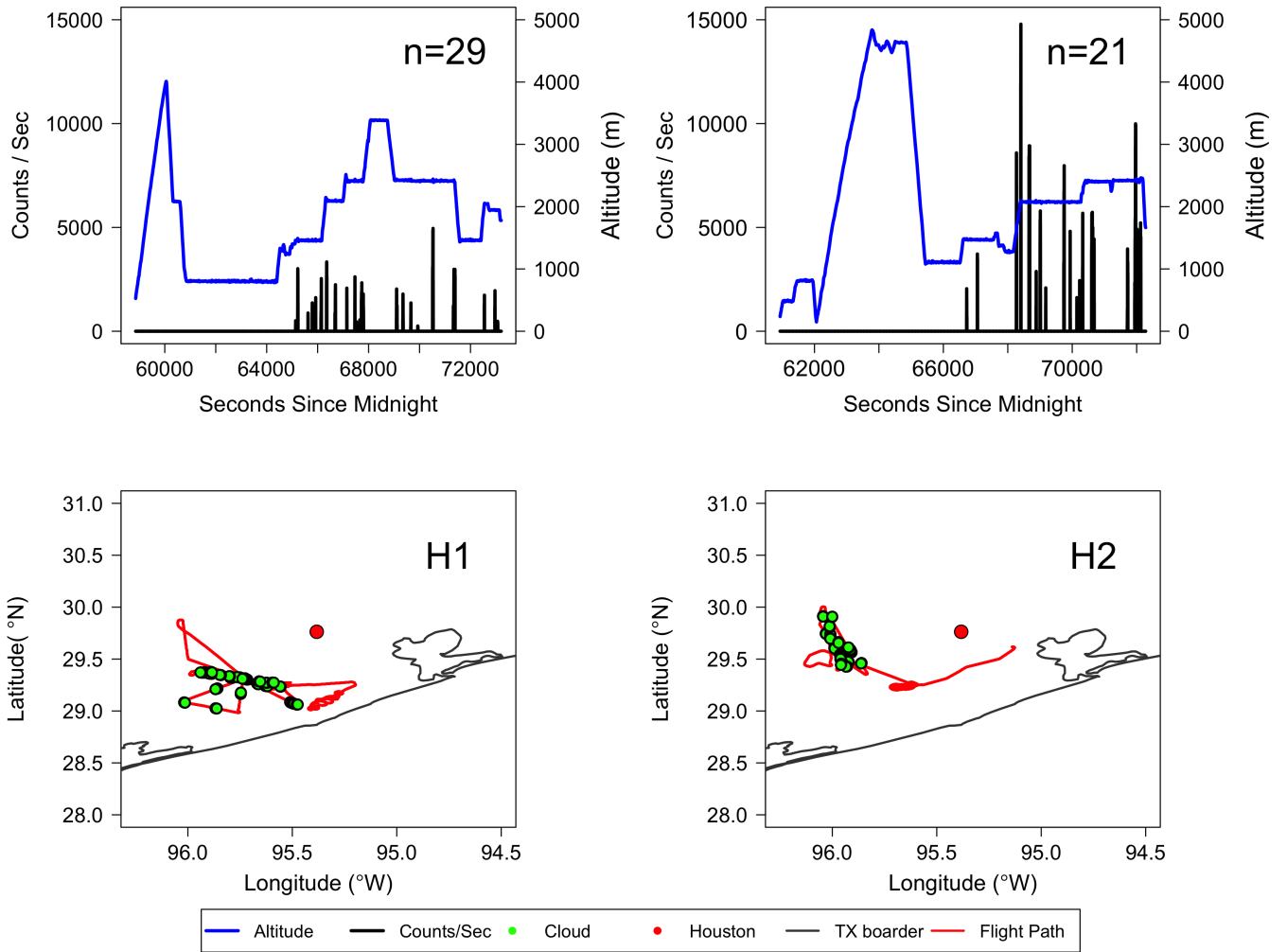


**Figure 3.** As in Figure 1, but for H1 and H2.

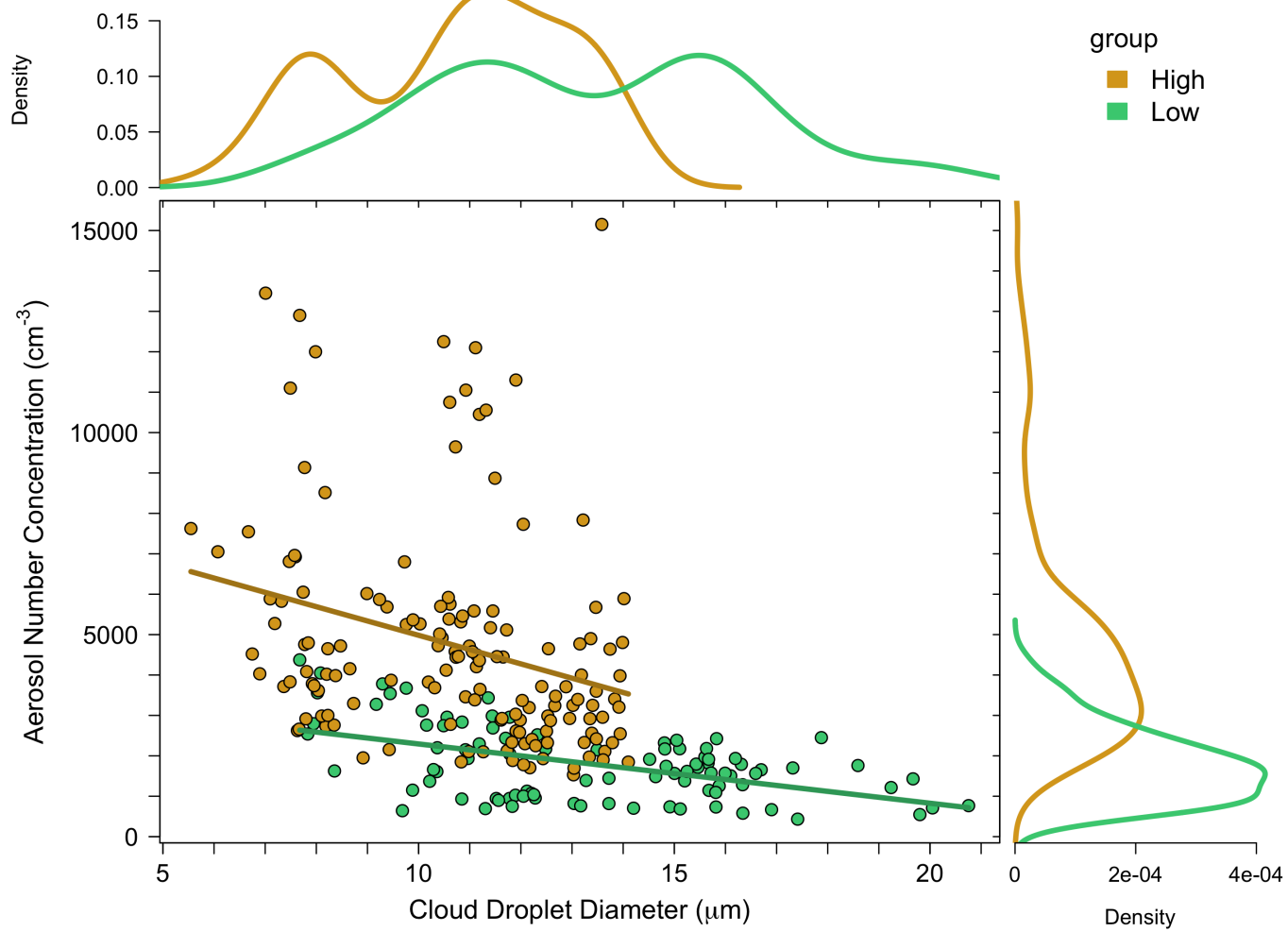


**Figure 4.** Shows cloud droplet diameter ( $\mu\text{m}$ ) on the x-axis and aerosol number concentration ( $\text{cm}^{-3}$ ) on the y-axis, with low pollution data in green and high pollution data in gold. The corresponding density curves of the high and low pollution data are given on the outer margins of the plot.

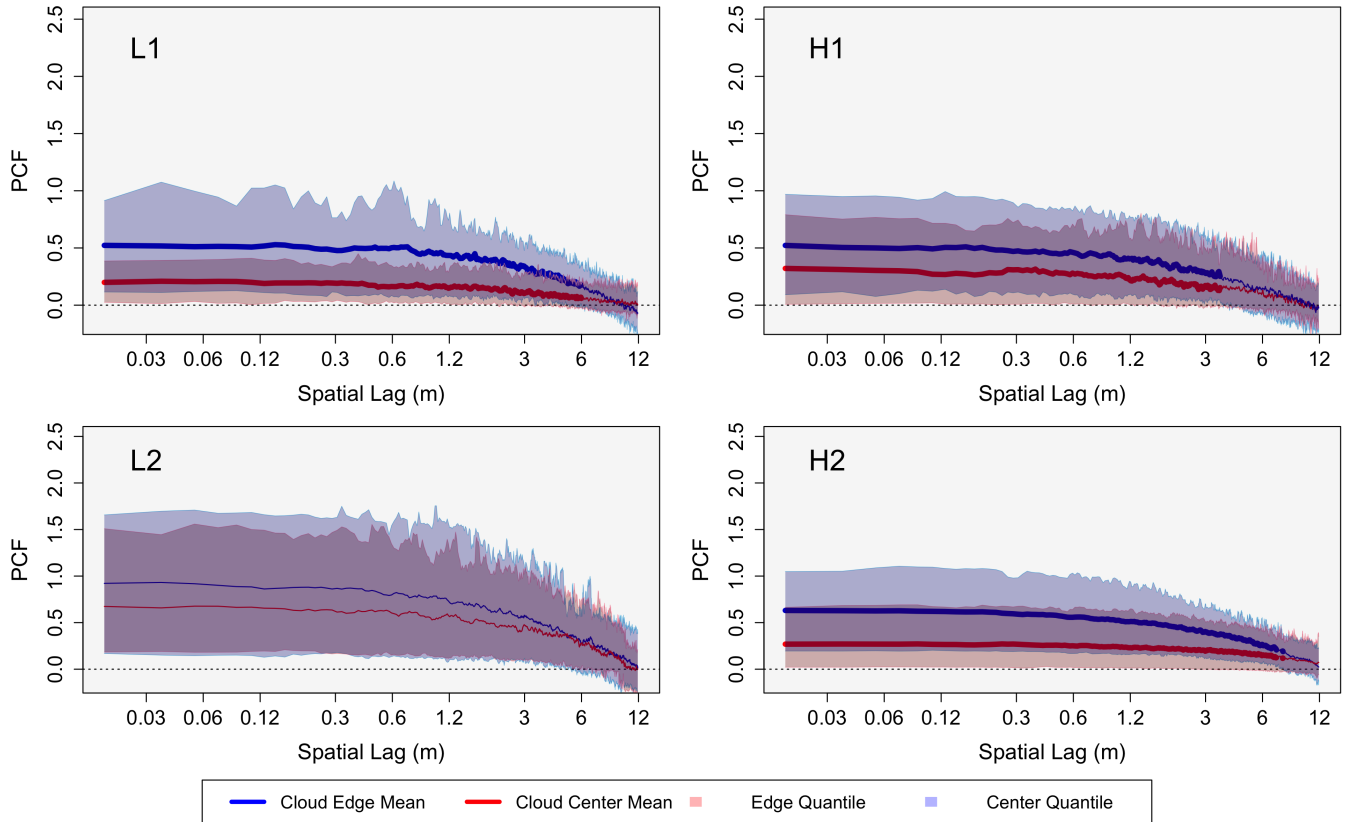
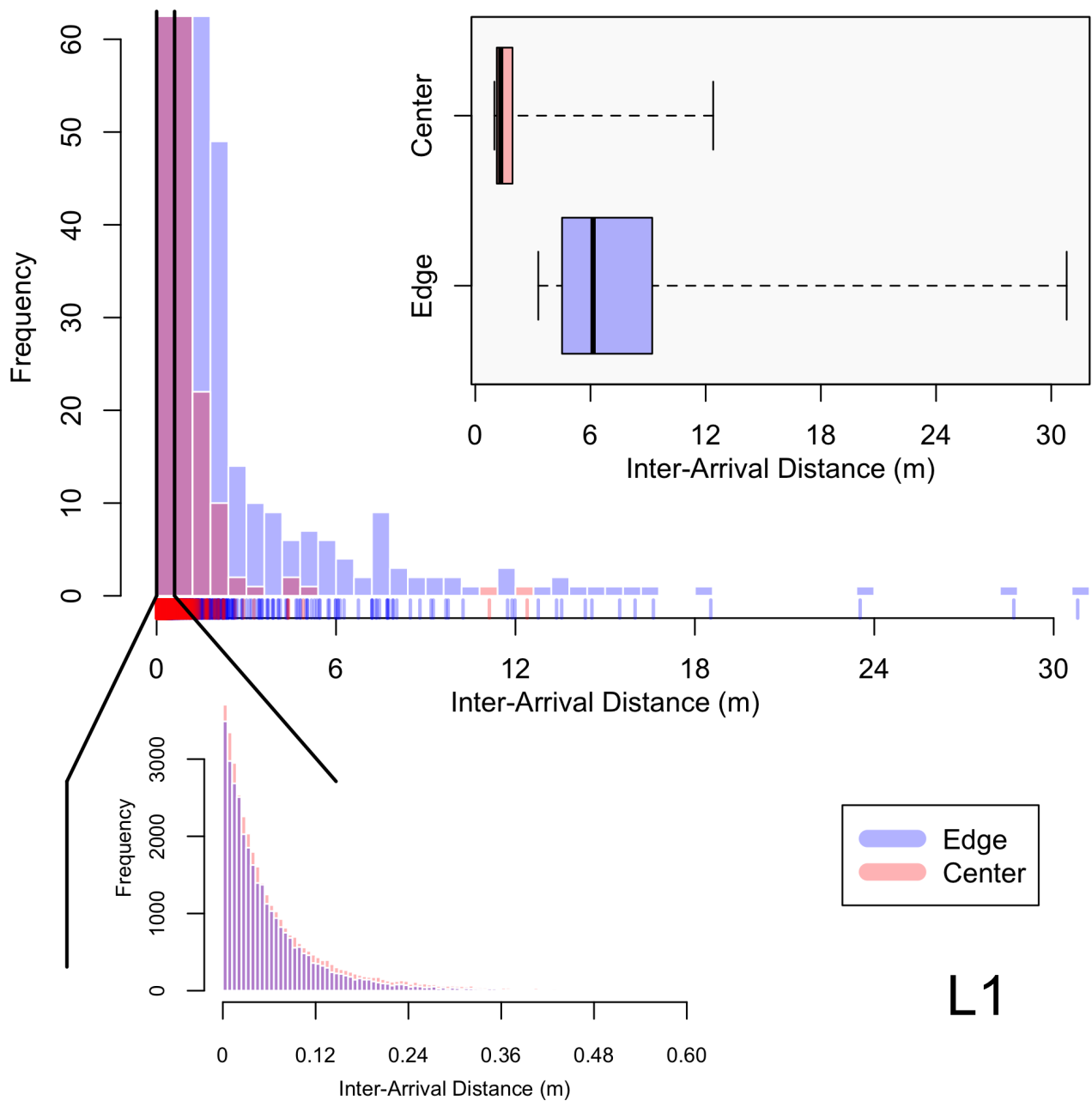


**Figure 5.** PCF clustering signatures for L1 (top right), L2 (bottom left), H1 (top right), and H2 (bottom right) with spatial lag (m) on the x-axis and PCF values (unitless) on the y-axis. **edge entrainment** data is in blue and cloud center data is in red, with the envelopes representing the 85<sup>th</sup> (top) and 15<sup>th</sup> (bottom) percent quantile values of the data. The mean PCF value for each case is represented by the middle line in each envelope, where a bold mean line represents **edge entrainment** and center differences that are statistically significant.



L1

**Figure 6.** Histogram distributions of the inter-arrival distance (IAD) for droplet populations measured in flight L1, with **edge entrainment** data in blue and center data in red. Note that the main histogram is zoomed in to a value of 60 on the y-axis, with further analysis of the first bin (representing a range from 0 to 0.60 m) below the main histogram. The boxplots in the top right represents the IAD data that is  $\geq$  the 0.998 quantile of the overall data sets for entrainment and center.

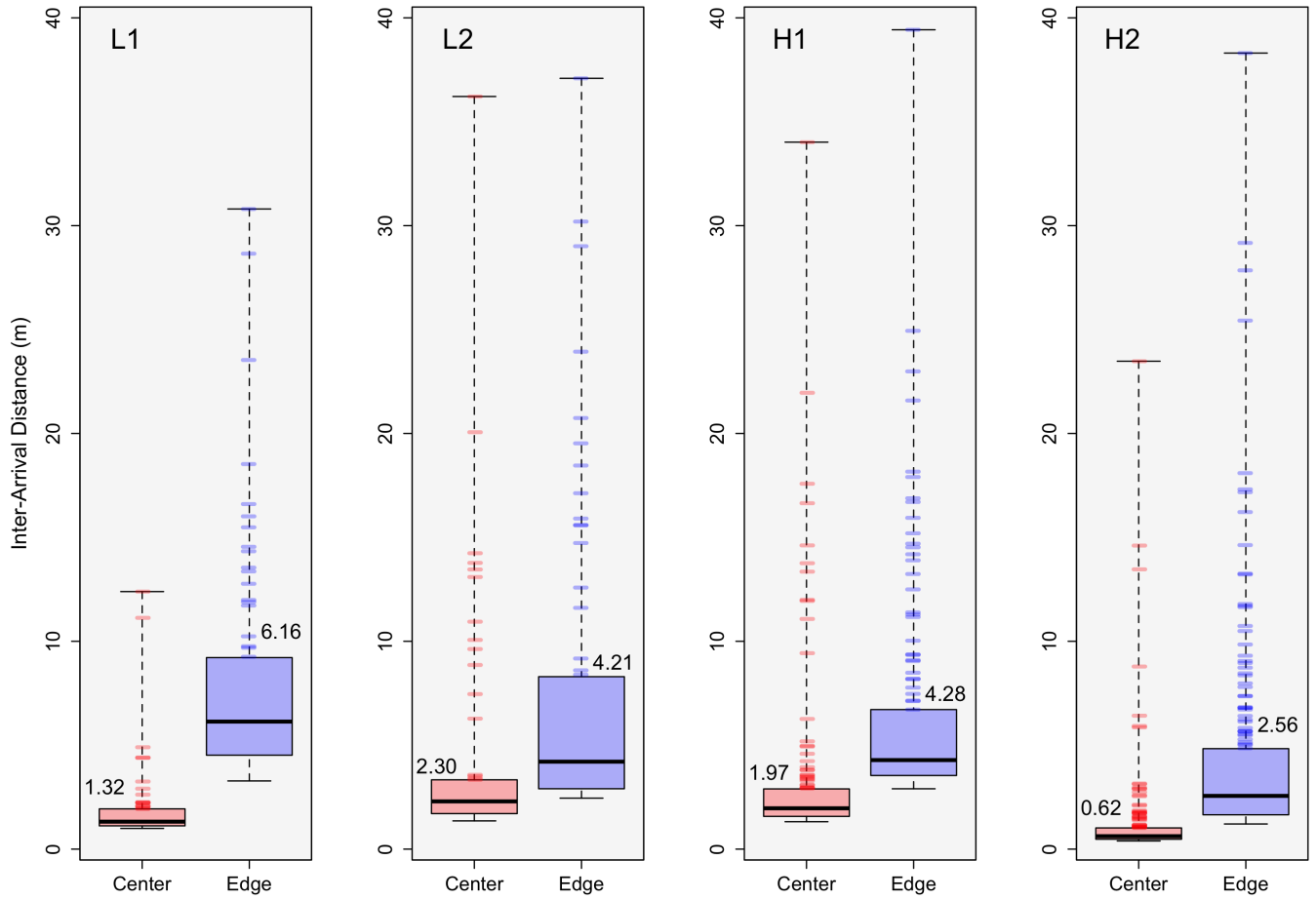


**Figure 7.** Boxplots for the IAD data which is  $\geq$  the 0.998 quantile of the overall data sets for **edge entrainment** (blue) and center (red), with L1, L2, H1, and H2 shown moving from left to right, respectively.

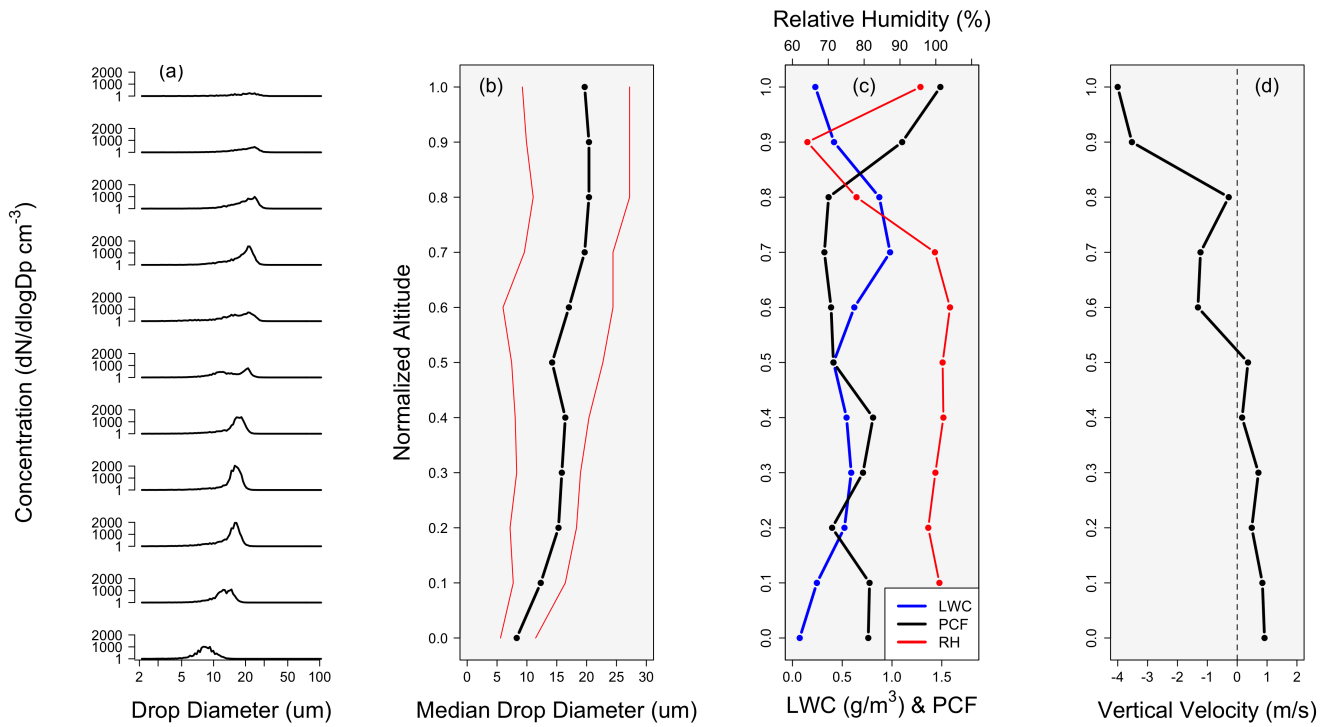


**Figure 8.** Shows the cloud droplet size distribution in panel (a). Panel (b) gives the median droplet size along with the 5<sup>th</sup> and 95<sup>th</sup> percent quantiles (red) of the droplet size distribution. Panel (c) shows LWC (blue), RH (red), and the PCF (black). Panel (d) shows vertical velocity. All variables are represented as a function of cloud normalized altitude.

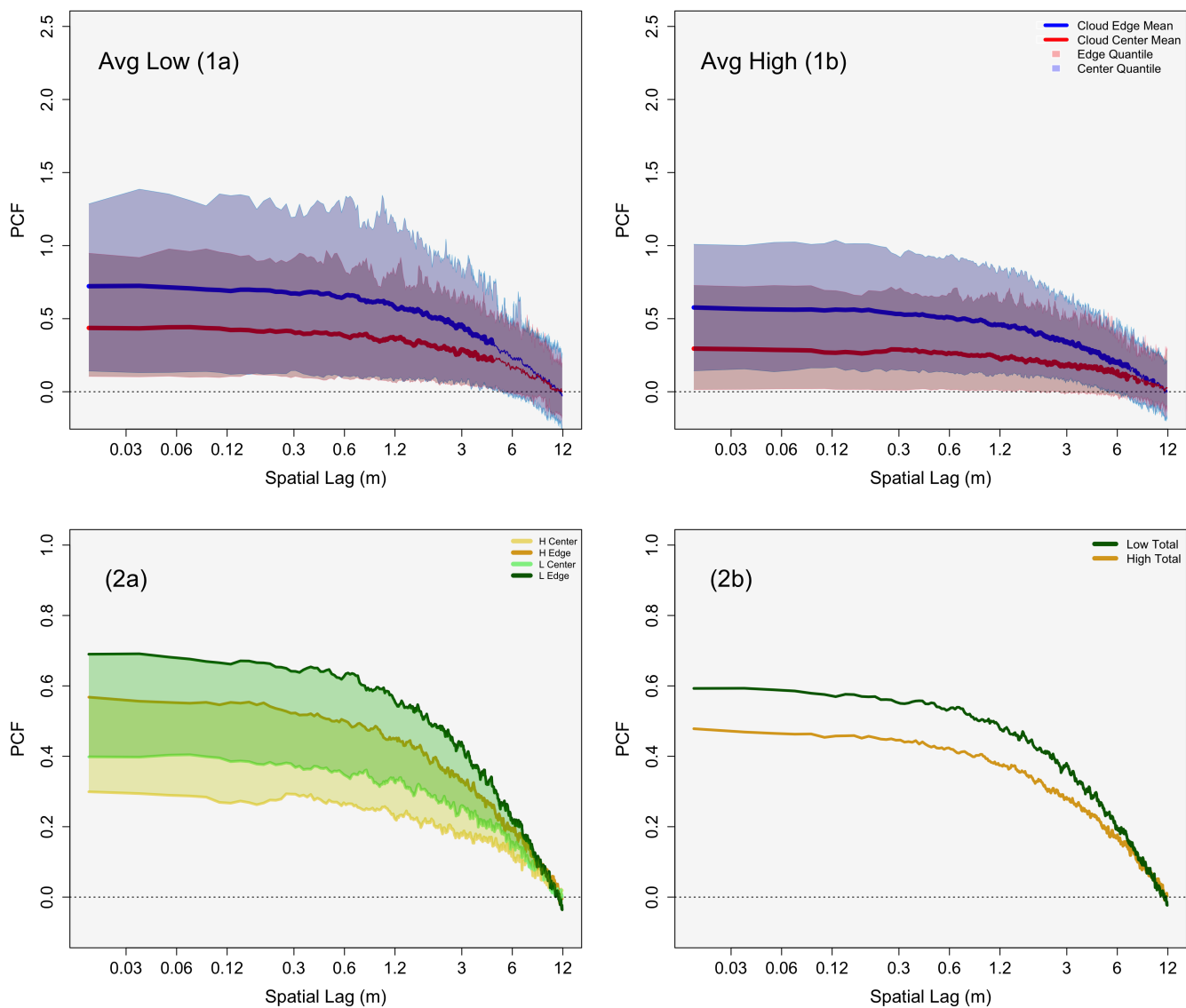


**Figure 9.** Panels (1a) and (1b): as in Figure 5, except for average low pollution PCF values (L1, L2) in Panel (1a) and average high pollution PCF values (H1, H2) in Panel (1b). Panels (2a) and (2b): low pollution data in green and high pollution data in gold. Panel (2a) shows envelopes that span the average center PCF value (lower limit of the envelopes) to the average edge entrainment PCF value (upper limit of the envelopes). Panel (2b) gives the overall average PCF value for low and high pollution clouds.

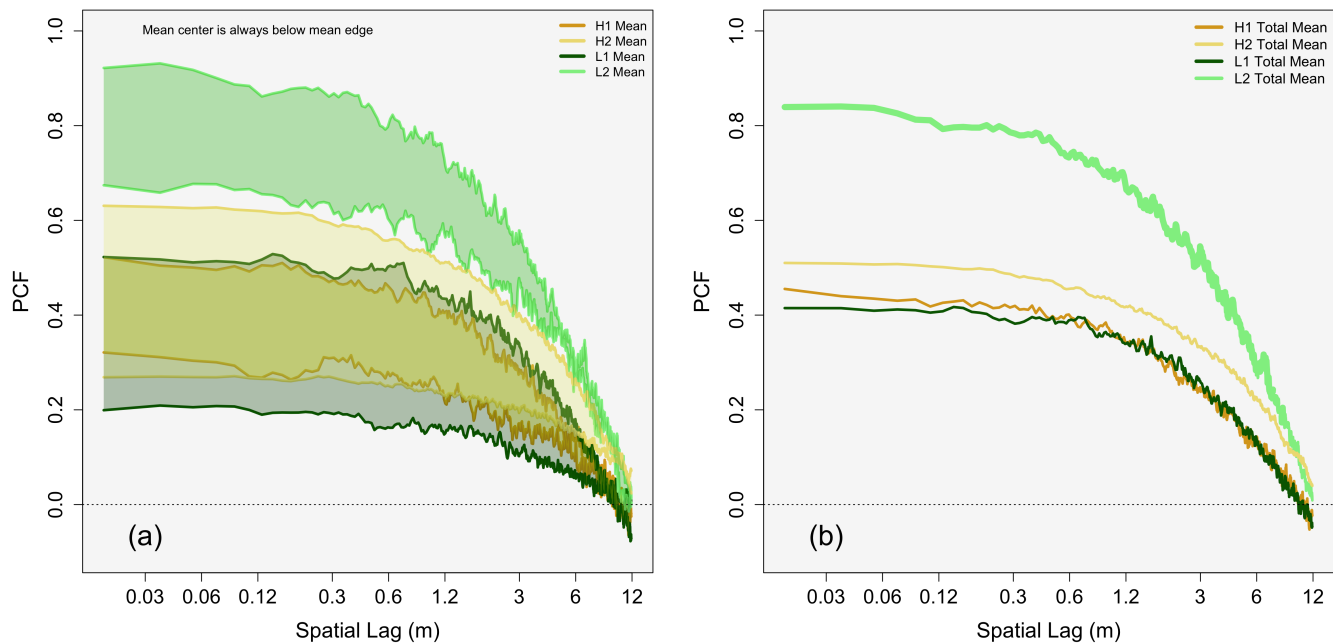


**Figure 10.** As in Panels (2a) and (2b) from Figure 9, except for the individual flights of L1 (dark green), L2 (light green), H1 (dark gold), and H2 (light gold). Note that the envelopes in Panel (a) represents the range from the mean center clustering (lower limit of each envelope) to the mean **edge entrainment** clustering (upper limit of each envelope).

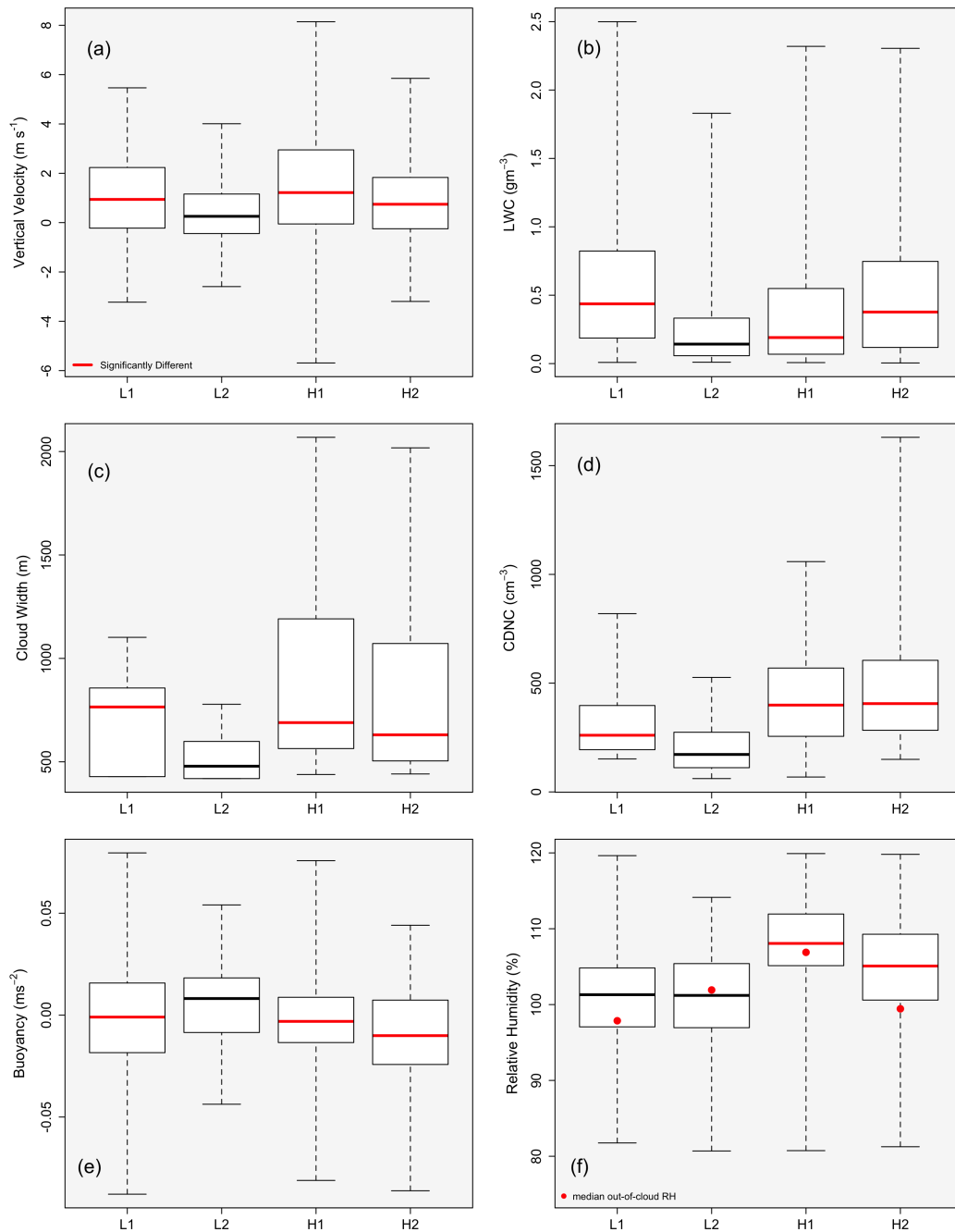


**Figure 11.** Box plots of L1, L2, H1, and H2, represented in that order on the x-axis, with Panels (a) through (f) representing vertical velocity ( $\text{m s}^{-1}$ ), LWC ( $\text{g m}^{-3}$ ), cloud width (m), CDNC ( $\text{cm}^{-3}$ ), buoyancy ( $\text{m s}^{-2}$ ), and in-cloud RH (%), respectively. Red median lines represent datasets that are statistically significant as compared to the L2 dataset. Each red dot in Panel (f) represents out-of-cloud RH.

**Table 1.** Shows the flight information for 20 of the 22 flights that occurred during the GoMACCS campaign. Each flight corresponds to a RF number, date, the number of clouds (after filtering, see text), the total aerosol number concentration ( $N_a$ ), and the accumulation mode aerosol number concentration ( $N_{acc}$ ). Values in parentheses represent the standard deviation.

RF Number	Date	Clouds	$N_a$ cm <sup>-3</sup>	$N_{acc}$ cm <sup>-3</sup>
1	8/21/06	1	NA	NA
2	8/22/06	11	NA	NA
3	8/23/06	9	2984 (588)	413 (66)
4	8/25/06	17	22667 (10672)	1797 (4184)
5	8/26/06	18	1304 (699)	290 (223)
6	8/27/06	0	NA	NA
7	8/28/06	0	NA	NA
9	8/29/06	28	3157 (1980)	360 (169)
11	8/31/06	37	3205 (650)	972 (214)
12	9/2/06	29	4768 (2826)	710 (169)
13	9/3/06	0	NA	NA
14	9/4/06	14	2770 (758)	697 (126)
15	9/6/06	10	1427 (398)	465 (147)
16	9/7/06	32	3547 (966)	949 (306)
17	9/8/06	21	4824 (1806)	821 (154)
18	9/10/06	1	1396 (918)	943 (472)
19	9/11/06	27	6561 (5419)	1280 (4172)
20	9/13/06	0	NA	NA
21	9/14/06	25	2230 (1157)	653 (276)
22	9/15/06	13	2323 (688)	436 (159)

**Table 2.** A summary of cloud, flight, and environmental properties from the L1, L2, H1, H2, and Case flights. Note that CDNC stands for cloud droplet number concentration, LWC stands for liquid water content, and Mean Drops ( $s^{-1}$ ) represents the mean number of drops measured by the PDI per second. Standard deviation values are represented in parentheses.

Variable	L1	L2	H1	H2	Case
Date	2006–Aug–26	2006–Sept–15	2006–Sept–02	2006–Sept–06	2006–Sept–10
Flight Number	RF 5	RF 22	RF 12	RF 17	RF 18
UTC for Cloud Sampling	1447–1717	1654–1748	1806–2018	1832–2002	1633–1742
Clouds > 300 m in width	18	13	29	21	1
Min cloud base height (m)	672	1120	1457	1476	806
Max cloud top height (m)	2412	2101	2463	2451	3381
Cloud thickness (m)	1740	981	1007	976	2575
Cloud width (m)	700 (235)	520 (110)	850 (404)	861 (451)	943 (472)
Mean true air speed ( $m s^{-1}$ )	61.2 (1.5)	59.9 (1.3)	62.7 (2.3)	63.0(2.3)	61.4 (2.2)
Mean CDNC ( $cm^{-3}$ )	318 (163)	210 (141)	421 (255)	531(363)	472 (404)
Max CDNC ( $cm^{-3}$ )	819	526	1059	1630	2342
Mean drops ( $s^{-1}$ )	661 (448)	1016 (1037)	958 (895)	3300 (2704)	1679 (1441)
Cloud top LWC ( $g m^{-3}$ )	0.97 (0.66)	0.55 (0.54)	0.47 (0.48)	0.60 (0.48)	0.45 (0.35))
Mean vertical velocity ( $m s^{-1}$ )	1.81 (1.67)	1.16 (1.28)	2.34 (2.21)	1.61 (1.62)	0.35 (1.89)
$N_a$ ( $cm^{-3}$ )	1304 (699)	2323 (688)	4768 (2826)	4824 (1806)	1396 (918)
$N_{acc}$ ( $cm^{-3}$ )	290 (223)	436 (159)	710 (169)	821 (154)	943 (472)
Environmental lapse rate ( $^{\circ}C km^{-1}$ )	5.4	4.5	4.8	5.7	NA
Environmental RH (%)	77	105	74	86	NA

**Table 3.** Average values for low (L1, L2) and high (H1, H2) pollution clouds for select variables from Table 2

Variable	Low	High
Mean CDNC ( $cm^{-3}$ )	264	476
Mean Drops ( $s^{-1}$ )	839	2129
$N_a$ ( $cm^{-3}$ )	1814	4796
$N_{acc}$ ( $cm^{-3}$ )	363	766
Cloud thickness (m)	1361	992
Cloud width (m)	610	856
Clouds > 300 m in width	31 (total)	50 (total)

**Table 4.** Provides the mean PCF, 85<sup>th</sup> percent quantile and 15<sup>th</sup> percent quantile values for center data (on the left) and **edge entrainment** data (on the right) for L1, L2, H1, and H2 in Figure 5, along with average low and high values from Figure 9

Flight	Center Data			Edge Data		
	Mean PCF	Upper Quantile	Lower Quantile	Mean PCF	Upper Quantile	Lower Quantile
<b>L1</b>	0.18	0.36	0.02	0.49	0.89	0.09
<b>L2</b>	0.61	1.39	0.16	0.83	1.62	0.14
<b>Avg. Low</b>	0.39	0.88	0.09	0.66	1.26	0.11
<b>H1</b>	0.26	0.69	0.009	0.46	0.86	0.09
<b>H2</b>	0.26	0.65	0.02	0.57	1.01	0.18
<b>Avg. High</b>	0.27	0.67	0.01	0.52	0.93	0.14

**Table 5.** Provides the mean p-value and the percent of data that is statistically significant (for the first 60 PCF values) between **edge entrainment** and center data for L1, L2, H1, and H2 in Figure 5 and for Average Low and High in Figure 9

Flight	p-value	% Significant
<b>L1</b>	$5.9 \cdot 10^{-3}$	100
<b>L2</b>	0.40	0
<b>Avg. Low</b>	0.01	100
<b>H1</b>	0.01	100
<b>H2</b>	$3.5 \cdot 10^{-4}$	100
<b>Avg. High</b>	$3.1 \cdot 10^{-5}$	100

**Table 6.** Provides the percentage of clustering that is significant and non-significant (as compared to a randomly distributed droplet population) for center (C) and **edge entrainment** (E) data in L1, L2, H1, and H2.

Flight	% Significant	% Non-significant
<b>L1 C</b>	44.4	55.5
<b>L1 E</b>	61.1	38.9
<b>L2 C</b>	92.3	7.7
<b>L2 E</b>	76.9	23.1
<b>H1 C</b>	48.3	51.7
<b>H1 E</b>	58.6	41.4
<b>H2 C</b>	71.4	28.6
<b>H2 E</b>	97.6	2.4

**Table 7.** Gives values for vertical velocity ( $\text{m s}^{-1}$ ), RH (%), LWC ( $\text{g m}^{-3}$ ), the PCF, and the median drop size ( $\mu\text{m}$ ), respectively, for each normalized cloud height in Figure 8

Normalized height	Vertical Velocity ( $\text{m s}^{-1}$ )	RH (%)	LWC ( $\text{g m}^{-3}$ )	PCF	Median drop size ( $\mu\text{m}$ )
0	0.91	100.38	0.07	0.76	8.29
0.1	0.84	101.01	0.24	0.77	12.32
0.2	0.49	97.89	0.52	0.40	15.29
0.3	0.71	99.88	0.59	0.71	15.85
0.4	0.16	102.12	0.54	0.81	16.43
0.5	0.36	101.90	0.41	0.41	14.23
0.6	-1.31	103.96	0.62	0.39	17.03
0.7	-1.22	99.74	0.98	0.32	19.67
0.8	-0.28	77.87	0.87	0.36	20.39
0.9	-3.52	64.17	0.41	1.10	20.37
1	-4.00	95.72	0.22	1.49	19.67

**Table 8.** Provides the mean p-value and the percent of data that is statistically significant (for the first 60 PCF values) between PCF functions provided in Panel (b) of Figure 10.

Comparison	p-value	% Significant
<b>L2-L1</b>	$2.2 \cdot 10^{-3}$	100
<b>L2-H1</b>	$1.3 \cdot 10^{-3}$	100
<b>L2-H2</b>	$2.2 \cdot 10^{-2}$	100
<b>L1-H1</b>	0.86	0
<b>L1-H2</b>	0.21	0
<b>H1-H2</b>	0.19	0

**Table 9.** Median values of vertical velocity ( $\text{m s}^{-1}$ ), LWC ( $\text{g m}^{-3}$ ), cloud width (m), CDNC ( $\text{cm}^{-3}$ ), buoyancy ( $\text{m s}^{-2}$ ), in-cloud RH and out-of-cloud RH (%) from Figure 11.

Variable Median	L1	L2	H1	H2
Vertical velocity ( $\text{m s}^{-1}$ )	0.94	0.25	1.21	0.74
LWC ( $\text{g m}^{-3}$ )	0.43	0.14	0.19	0.38
Cloud width (m)	765	480	690	631
CDNC ( $\text{cm}^{-3}$ )	261	172	399	406
Buoyancy ( $\text{m s}^{-3}$ )	-0.00097	0.0081	-0.0031	-0.010
in-cloud RH	101.3	101.2	108.1	105.1
out-of-cloud RH	97.8	101.9	106.8	99.4

**Table 10.** Gives p-values between L2 and L1, L2 and H1, and L2 and H2 for in-cloud vertical velocity ( $\text{m s}^{-1}$ ), LWC ( $\text{g m}^{-3}$ ), RH (%), CDNC ( $\text{cm}^{-3}$ ), cloud width (m), and in-cloud buoyancy ( $\text{m s}^{-2}$ ). Statistically significant values are presented in bold.

Comparison	Vertical Velocity (m/s)	LWC $\text{gm}^{-3}$	RH (Percent)	CDNC ( $\text{cm}^{-3}$ )	Width (m)	Buoyancy ( $\text{ms}^{-2}$ )
L2-L1	<b><math>6.0 \cdot 10^{-4}</math></b>	<b><math>2.1 \cdot 10^{-12}</math></b>	0.82	<b>0.03</b>	<b>0.008</b>	<b>0.011</b>
L2-H1	<b><math>2.9 \cdot 10^{-7}</math></b>	<b>0.009</b>	$< 2.2 \cdot 10^{-16}$	<b>0.002</b>	<b><math>7.8 \cdot 10^{-4}</math></b>	<b><math>3.9 \cdot 10^{-5}</math></b>
L2-H2	<b>0.011</b>	<b><math>2.2 \cdot 10^{-7}</math></b>	<b><math>3.87 \cdot 10^{-7}</math></b>	<b><math>1.9 \cdot 10^{-4}</math></b>	<b>0.003</b>	<b><math>5.5 \cdot 10^{-11}</math></b>